Limited circulation. For review only
IEEE TCST Submission no.: 21-0322.1

Load and Renewable-Following Control of Linearization-Free Differential Algebraic Equation Power System Models

Sebastian A. Nugroho*, *IEEE, Student Member* and Ahmad F. Taha†, *IEEE, Member*

***Abstract*—Electromechanical transients in power networks are mostly caused by mismatch between power consumption and production, causing generators to deviate from the nominal frequency. To that end, feedback control algorithms have been designed to perform frequency and load/renewables-following control. In particular, the literature addressed a plethora of grid- and frequency-control challenges with a focus on linearized, differential equation models whereby algebraic constraints (i.e., power flows) are eliminated. This is in contrast with the more realistic nonlinear differential algebraic equation (NDAE) models. Yet, as grids are increasingly pushed to their limits via intermittent renewables and varying loads, their physical states risk escaping operating regions due to either a poor prediction or sudden changes in renewables or demands—deeming a feedback controller based on a linearization point virtually unusable. In lieu of linearized differential equation models, the objective of this paper is to design a simple, purely decentralized, linearization-free, feedback control law for NDAE models of power networks. The objective of such controller is to primarily stabilize frequency oscillations after a large, unknown disturbance in renewables or loads. Although the controller design involves advanced NDAE system theory, the controller itself is as simple as a decentralized proportional or linear quadratic regulator in its implementation. Case studies demonstrate that the proposed controller is able to stabilize dynamic and algebraic states under significant disturbances.**

***Keywords*—Load following control, frequency regulation, power networks, differential-algebraic equations.**

I. Introduction

OVER the years, the trends of global electricity generation has been shifting from fuel-based conventional generators to a mix of such type with fuel-free renewable energy resources such as wind and PV solar farms. Nowadays, renewable energy sources contribute around 21% of the total generated electricity in the U.S. and it is projected that their contribution will double to 42% by 2050 [1]. Albeit the increasing penetration of renewables in bulk power systems plays a vital role in mitigating climate change [2], it unfortunately presents a major challenge in power systems operation due to the intermittent and uncertain nature of renewables and loads. This challenge is met by two main goals in power systems control which are *(i)* maintaining the balance between power supply and demand while also *(ii)* preserving the systems-wide frequency [3]. Both objectives are essential to achieve successful power systems operation as significant power imbalance and large frequency deviation can provide adverse impacts which can eventually result in system collapse [4].

The increasing penetration of renewables makes the aforementioned tasks to be remarkably difficult to achieve and with that in mind, this paper is dedicated to address the problem of *load and renewable-following control* (LRFC), which focus is preserving the power balance and system's frequency against unpredictable behavior of power demand and renewables. This problem is closely related to the *load following control* (LFC), in which power imbalance and frequency deviations are mainly attributed to changes in power demand only [5]. There exist numerous methods to address the problem pertaining to LFC. In multi-area power networks, automatic generation control (AGC) is a secondary, inter-area control architecture which purpose is regulating the network's frequency and interchange of power flow [6]. Other than AGC, many proportional-integral-derivative (PID)-based controllers have also been proposed in the literature. Methods that are based on PID can be categorized into internal model control, fractional order method, soft computing approach, and robust control scheme [7]. Although PID is known for its simplicity, it unfortunately requires rigorous tuning and the results based on conventional approaches are often not generally robust [7].

The shortcomings of conventional AGC and PID controllers motivate the development of advanced control techniques, particularly for power network applications. The advancement of convex optimization theory as well as computational method facilitates the design of linear matrix inequalities (LMIs)-based stabilization. Advanced control strategies for power networks—albeit are not limited solely for LFC—can be generally categorized into *(a)* unified, wide-area control and *(b)* localized, decentralized control frameworks. Related to the wide-area control, the authors in [8], [9], and [10] respectively employ the adaptive control, linear quadratic Gaussian control, and model predictive control frameworks to minimize power oscillations and improve damping between multiple areas. Since most of these methods result in a centralized control laws that may not be suitable for large-scale networks, a new optimization-based method is developed in [11] to synthesize a sparse optimal control policy.

The study [12] combines the optimal power flow problem with LFC using linear quadratic regulator (LQR). Recently, a method developed using the notion of $\mathcal{L}_\infty$ stability is proposed in [13] to implement a robust control architecture for LRFC in power systems. The behavior of power networks with respect to the increasing penetration of distributed energy resources (DERs) including renewables is investigated in [14], where it

*Department of Electrical Engineering and Computer Science, University of Michigan, 1301 Beal Ave., Ann Arbor, MI 48109 (snugroho@umich.edu).
†Department of Civil and Environmental Engineering, Vanderbilt University, 2201 West End Ave., Nashville, TN 37235 (ahmad.taha@vanderbilt.edu).
This work is partially supported by Valero Energy Corporation and National Science Foundation under Grant 2044430 and 2013786.

is revealed that the increasing number of DERs connected to the network can reduce the system's stability. All of the aforementioned studies rely on the *linearized* ordinary differential equations (ODEs) model of power networks. The drawbacks of this approach are: *(i)* the linearization and controller synthesis need to be performed periodically while *(ii)* the resulting control law can only stabilize the system in a small operating region.

For the decentralized grid control architecture, [15], [16] pioneer the design of robust decentralized stabilization for interconnected multi-machine power networks modeled as *nonlinear* ODEs. The underlying concept behind this approach is to treat the nonlinearities of the system as a source of uncertainty and as such, provided that these nonlinearities are quadratically bounded, a linear state feedback control gain can be synthesized by solving convex optimization problems with LMIs. This idea has been utilized in [17], [18] and later on is extended to enhance power networks' transient dynamics [6], improve damping in inter-area oscillations [19], and tackle parametric uncertainties via $\mathcal{H}_\infty$ control [20]. In addition to this, a decentralized control based on the LQR for improving small signal stability and providing a sufficient damping is proposed in [21]. Albeit the methods proposed in [6], [15], [16], [19] are not relying on any linearization either, they *(i)* only consider active power transfer between generators and loads, *(ii)* the model is valid only for the reduced network (only comprised of generator buses), and *(iii)* the disturbance due to renewables uncertainty is not taken into consideration.

To circumvent the limitations from these approaches, efforts have been made recently to study the properties as well as stability of power systems based on their differential-algebraic equation (DAE) models. For instance, [22] studies the structural properties of the *linearized* DAE model of power networks—this is extended in [23] to include higher order generator dynamics. Utilizing the model presented in [22], the author in [24] presents a condition to determine the small signal stability of power networks. Moreover, the problem of characterizing topological changes in linear DAE systems is investigated in [25]. The main advantage of using the DAE representation of power networks relative to ODE is that the behavior of the network's dynamics can be tightly linked with the network's topology and power flow equations. Besides, if the nonlinear DAE (NDAE) models are considered, the dynamical behavior of the system can be studied across wider operating regions while regulating both the algebraic and dynamic variables in a power system. These altogether allow a more thorough and realistic study of power systems to be performed.

Motivated by the drawbacks existing in previous studies, herein we propose a novel approach for LRFC by leveraging the classical NDAE models of power networks. The LRFC is derived based on a more comprehensive 4$^{\text{th}}$-order generator dynamic model, complete with generator's complex power and power balance equations. To the best of our knowledge, this is the first attempt to provide a secondary control based on the NDAE models of multi-machine power networks. The proposed LRFC strategy is intended to maintain network's frequency, which variability is attributed to a sudden change in power demand and power produced by renewable energy resources. The paper's contributions include:

- The introduction of a new state feedback control framework for LRFC using a detailed, high-order NDAE model of power networks. The proposed LRFC strategy does *not* require any linearization and as such, its gain-computation is not linked to any operating point. Moreover, the resulting state feedback gain matrix possesses a decentralized information structure. This *(i)* improves the practicality of the proposed LRFC especially for larger networks while *(ii)* eliminates the need for an optimization strategy to *sparsify* the controller's structure.
- The development of a convex optimization-based approach for the stabilization of NDAEs. Although the stability of NDAEs has been studied in the literature for quite some time (for example, see [26]–[28]), approaches for the stabilization of NDAEs based on LMIs are, unfortunately, still lacking. Hence, we propose herein a computationally friendly approach for the stabilization of NDAEs based on a simple state feedback control policy using LMIs. Later, the computed controller gain matrix can be used to perform LRFC.
- We showcase the effectiveness and performance of the proposed approach to perform LRFC. In addition, the proposed approach is compared with AGC and LQR-based control. Numerical test results indicate the superiority of our approach to perform LRFC relative to LQR and AGC, since it can maintain network's frequency and power balance subject to a relatively large disturbance.

The remainder of the paper is organized as follows. Section II, presents the semi-explicit, NDAE models of power networks while Section III discusses the design of the proposed state feedback control strategy for the stabilization of NDAEs, especially for LRFC. Thorough numerical studies are provided in Section IV; the results are discussed accordingly. Finally, the paper is concluded in Section V.

Notation. The notation $\mathbf{1}$ denotes a column vector with elements of 1 while $\boldsymbol{I}$ and $\boldsymbol{O}$ represent the identity and zero matrices of appropriate dimensions. The notations $\mathbb{R}^n$ and $\mathbb{R}^{p\times q}$ denote the sets of row vectors with n elements and matrices with size p-by-q with elements in $\mathbb{R}$. The operators $\text{Blkdiag}(\cdot)$ constructs a block diagonal matrix, $\text{Diag}(\cdot)$ constructs a diagonal matrix from a vector, $\oslash$ denotes the Hadamard division, and $\odot$ denotes the Hadamard product. The symbol $*$ represents symmetric entries in symmetric matrices.

II. Description of Power Network Dynamics

We consider a power network consisting N number of buses, modeled by a graph $(\mathcal{N},\mathcal{E})$ where $\mathcal{N}$ is the set of nodes and $\mathcal{E}$ is the set of edges. Note that $\mathcal{N}$ consists of traditional synchronous generator, renewable energy resources, and load buses, i.e., $\mathcal{N} = \mathcal{G}\cup\mathcal{R}\cup\mathcal{L}$ where $\mathcal{G}$ collects G generator buses, $\mathcal{R}$ collects the buses containing R renewables, while $\mathcal{L}$ collects L load buses. Readers are referred to Tab. I for the detailed description of the notations used in the modeling of the network. In this work, we leverage a 4$^{\text{th}}$-order dynamics of synchronous generators modeled as [13], [29]

$$\dot{\delta}_i = \omega_i - \omega_0 \tag{1a}$$

$$M_i\dot{\omega}_i = T_{\text{M}i} - P_{\text{G}i} - D_i(\omega_i-\omega_0) \tag{1b}$$

$$T'_{\text{d}0i}\dot{E}'_i = -\tfrac{x_{\text{d}i}}{x'_{\text{d}i}}E'_i + \tfrac{x_{\text{d}i}-x'_{\text{d}i}}{x'_{\text{d}i}}v_i\cos(\delta_i-\theta_i) + E_{\text{fd}i} \tag{1c}$$

Table I
DESCRIPTION OF IMPORTANT NOTATIONS USED IN THIS PAPER.

Notation	Description
$\mathcal{N} := \{1, 2, \ldots, N\}$	set of nodes (buses)
$\mathcal{E} \subseteq \mathcal{N} \times \mathcal{N}$	set of edges (links)
$\mathcal{G} := \{1, 2, \ldots, G\}$	set of generator buses
$\mathcal{R} := \{1, 2, \ldots, R\}$	set of buses with renewables
$\mathcal{L} := \{1, 2, \ldots, L\}$	set of load buses
$\delta_i := \delta_i(t)$	generator rotor angle (rad)
$\omega_i := \omega_i(t)$	generator rotor speed (rad/sec)
$E'_i := E'_i(t)$	generator transient voltage (pu)
$T_{\mathrm{M}i} := T_{\mathrm{M}i}(t)$	generator mechanical input torque (pu)
$E_{\mathrm{fd}i} := E_{\mathrm{fd}i}(t)$	generator internal field voltage (pu)
$T_{\mathrm{r}i} := T_{\mathrm{r}i}(t)$	governor reference signal (pu)
M_i	rotor inertia constant (pu $\times$ sec^2)
D_i	damping coefficient (pu $\times$ sec)
$x_{\mathrm{d}i}$	direct-axis synchronous reactance (pu)
$x_{\mathrm{q}i}$	direct-axis synchronous reactance (pu)
$x'_{\mathrm{d}i}$	direct-axis transient reactance (pu)
$T'_{\mathrm{d0}i}$	direct-axis open-circuit time constant (sec)
$T_{\mathrm{CH}i}$	chest valve time constant (sec)
$R_{\mathrm{D}i}$	speed governor regulation constant (Hz/pu)
ω_0	synchronous speed ($2\pi 60$ rad/sec)
$P_{\mathrm{G}i},\ Q_{\mathrm{G}i}$	generator's active and reactive power (pu)
$P_{\mathrm{R}i},\ Q_{\mathrm{R}i}$	renewable's active and reactive power (pu)
$P_{\mathrm{L}i},\ Q_{\mathrm{L}i}$	load's active and reactive power (pu)
$\bar{v}_i = v_i e^{j\theta_i}$	complex bus voltage (pu)
$\boldsymbol{x}_d \in \mathbb{R}^{n_d}$	dynamic states
$\boldsymbol{x}_a \in \mathbb{R}^{n_a}$	algebraic states
$\boldsymbol{u} \in \mathbb{R}^{n_u}$	system's overall inputs
$\boldsymbol{q} \in \mathbb{R}^{n_q}$	demand and renewables generation

$$T_{\mathrm{CH}i}\dot{T}_{Mi} = -T_{\mathrm{M}i} - \tfrac{1}{R_{\mathrm{D}i}}(\omega_i - \omega_0) + T_{\mathrm{r}i}. \tag{1d}$$

The time-varying components in (1) include: generator's internal states δ_i, ω_i, E'_i, $T_{\mathrm{M}i}$; generator's inputs $E_{\mathrm{fd}i}$, $T_{\mathrm{r}i}$. The relations among generator's internal states $(\delta_i, \omega_i, E'_i, T_{\mathrm{M}i})$, generator's supplied power $(P_{\mathrm{G}i}, Q_{\mathrm{G}i})$, and terminal voltage $\bar{v}_i$ are represented by two algebraic constraints below [13]

$$P_{\mathrm{G}i} = \tfrac{1}{x'_{\mathrm{d}i}} E'_i v_i \sin(\delta_i - \theta_i) - \tfrac{x_{\mathrm{q}i} - x'_{\mathrm{d}i}}{2x'_{\mathrm{d}i}x_{\mathrm{q}i}} v_i^2 \sin(2(\delta_i - \theta_i)) \tag{2a}$$

$$\begin{aligned} Q_{\mathrm{G}i} = {} & \tfrac{1}{x'_{\mathrm{d}i}} E'_i v_i \cos(\delta_i - \theta_i) - \tfrac{x'_{\mathrm{d}i} + x_{\mathrm{q}i}}{2x'_{\mathrm{d}i}x_{\mathrm{q}i}} v_i^2 \\ & - \tfrac{x_{\mathrm{q}i} - x'_{\mathrm{d}i}}{2x'_{\mathrm{d}i}x_{\mathrm{q}i}} v_i^2 \cos(2(\delta_i - \theta_i)). \end{aligned} \tag{2b}$$

The power flow/balance equations—which resemble the power transfer among generators, renewable energy resources, and loads—are given as follows [29]

$$P_{\mathrm{G}i} + P_{\mathrm{R}i} + P_{\mathrm{L}i} = \sum_{j=1}^{N} v_i v_j (G_{ij} \cos\theta_{ij} + B_{ij} \sin\theta_{ij}) \tag{3a}$$

$$Q_{\mathrm{G}i} + Q_{\mathrm{R}i} + Q_{\mathrm{L}i} = \sum_{j=1}^{N} v_i v_j (G_{ij} \sin\theta_{ij} - B_{ij} \cos\theta_{ij}), \tag{3b}$$

where $i \in \mathcal{G} \cap \mathcal{R} \cap \mathcal{L}$, $\theta_{ij} := \theta_i - \theta_j$, and (G_{ij}, B_{ij}) respectively denote the conductance and susceptance between bus i and j which can be directly obtained from the network's bus admittance matrix [29]. In the above equations, $(P_{\mathrm{R}i}, Q_{\mathrm{R}i})$ denote the active and reactive power generated by renewables, while

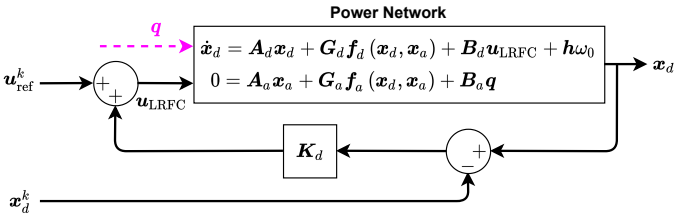

Figure 1. Control architecture for LRFC. Vector $\boldsymbol{q}$ denotes the actual demand and renewables generation which values are generally unknown.

$(P_{\mathrm{L}i}, Q_{\mathrm{L}i})$ denote the active and reactive power consumed by the loads. For the case at which a bus does not contain generator, renewable, and/or load, then the absence of one or more of these units can be indicated by setting its/their corresponding active and reactive power in (3) to zero. Now, let us define: $\boldsymbol{x}_d$ as the vector populating all dynamic states of the network such that $\boldsymbol{x}_d := \begin{bmatrix}\boldsymbol{\delta}^\top & \boldsymbol{\omega}^\top & \boldsymbol{E}'^\top & \boldsymbol{T}_{\mathrm{M}}^\top\end{bmatrix}^\top$ in which $\boldsymbol{\delta} := \{\delta_i\}_{i\in\mathcal{G}}$, $\boldsymbol{\omega} := \{\omega_i\}_{i\in\mathcal{G}}$, $\boldsymbol{E}' := \{E'_i\}_{i\in\mathcal{G}}$, $\boldsymbol{T}_{\mathrm{M}} := \{T_{\mathrm{M}i}\}_{i\in\mathcal{G}}$; $\boldsymbol{a}$ as the algebraic state corresponding to generator's power such that $\boldsymbol{a} := \begin{bmatrix}\boldsymbol{P}_{\mathrm{G}}^\top & \boldsymbol{Q}_{\mathrm{G}}^\top\end{bmatrix}^\top$ where $\boldsymbol{P}_{\mathrm{G}} := \{P_{\mathrm{G}i}\}_{i\in\mathcal{G}}$, $\boldsymbol{Q}_G := \{Q_{\mathrm{G}i}\}_{i\in\mathcal{G}}$; and $\tilde{\boldsymbol{v}}$ as the algebraic state representing the network's complex bus voltages such that $\tilde{\boldsymbol{v}} := \begin{bmatrix}\boldsymbol{v}^\top & \boldsymbol{\theta}^\top\end{bmatrix}^\top$ where $\boldsymbol{v} := \{v_i\}_{i\in\mathcal{N}}$, $\boldsymbol{\theta} := \{\theta_i\}_{i\in\mathcal{N}}$. The input of the system is considered to be $\boldsymbol{u} := \begin{bmatrix}\boldsymbol{E}_{\mathrm{fd}}^\top & \boldsymbol{T}_{\mathrm{r}}^\top\end{bmatrix}^\top$ where $\boldsymbol{E}_{\mathrm{fd}} := \{E_{\mathrm{fd}i}\}_{i\in\mathcal{G}}$ and $\boldsymbol{T}_{\mathrm{r}} := \{T_{\mathrm{r}i}\}_{i\in\mathcal{G}}$. In addition, define the vector $\boldsymbol{q}$ as $\boldsymbol{q} := \begin{bmatrix}\boldsymbol{P}_{\mathrm{R}}^\top & \boldsymbol{Q}_{\mathrm{R}}^\top & \boldsymbol{P}_{\mathrm{L}}^\top & \boldsymbol{Q}_{\mathrm{L}}^\top\end{bmatrix}^\top$ where $\boldsymbol{P}_{\mathrm{R}} := \{P_{\mathrm{R}i}\}_{i\in\mathcal{R}}$, $\boldsymbol{Q}_{\mathrm{R}} := \{Q_{\mathrm{R}i}\}_{i\in\mathcal{R}}$, $\boldsymbol{P}_{\mathrm{L}} := \{P_{\mathrm{L}i}\}_{i\in\mathcal{L}}$, $\boldsymbol{Q}_{\mathrm{L}} := \{Q_{\mathrm{L}i}\}_{i\in\mathcal{L}}$. Based on the constructed vectors described above, the state-space, NDAE model of multi-machine power networks (1)-(3) can be written as

$$\boxed{\begin{aligned} \dot{\boldsymbol{x}}_d &= \boldsymbol{A}_d\boldsymbol{x}_d + \boldsymbol{G}_d\boldsymbol{f}_d(\boldsymbol{x}_d, \boldsymbol{x}_a) + \boldsymbol{B}_d\boldsymbol{u} + \boldsymbol{h}\omega_0 && \text{(4a)} \\ \boldsymbol{0} &= \boldsymbol{A}_a\boldsymbol{x}_a + \boldsymbol{G}_a\boldsymbol{f}_a(\boldsymbol{x}_d, \boldsymbol{x}_a) + \boldsymbol{B}_a\boldsymbol{q}, && \text{(4b)} \end{aligned}}$$

where $\boldsymbol{x}_d \in \mathbb{R}^{n_d}$, $\boldsymbol{x}_a := \begin{bmatrix}\boldsymbol{a}^\top & \tilde{\boldsymbol{v}}^\top\end{bmatrix}^\top \in \mathbb{R}^{n_a}$, $\boldsymbol{u} \in \mathbb{R}^{n_u}$, and $\boldsymbol{q} \in \mathbb{R}^{n_q}$. The functions $\boldsymbol{f}_d : \mathbb{R}^{n_d} \times \mathbb{R}^{n_a} \to \mathbb{R}^{n_{fd}}$, $\boldsymbol{f}_a : \mathbb{R}^{n_d} \times \mathbb{R}^{n_a} \to \mathbb{R}^{n_{fa}}$, constant matrices $\boldsymbol{A}_d \in \mathbb{R}^{n_d \times n_d}$, $\boldsymbol{A}_a \in \mathbb{R}^{n_a \times n_a}$, $\boldsymbol{G}_d \in \mathbb{R}^{n_{fd} \times n_d}$, $\boldsymbol{G}_a \in \mathbb{R}^{n_{fa} \times n_a}$, $\boldsymbol{B}_d \in \mathbb{R}^{n_u \times n_d}$, $\boldsymbol{B}_a \in \mathbb{R}^{n_q \times n_a}$, and vector $\boldsymbol{h} \in \mathbb{R}^{n_d}$ are all detailed in Appendix A. In the ensuing sections, the development of a LRFC law $\boldsymbol{u}(t)$ for power networks modeled in (4) is presented.

III. STATE FEEDBACK CONTROL DESIGN FOR NDAEs

A. State Feedback Control Strategy for LRFC

The scheduling of synchronous generators in power networks is performed based on the loads and renewables demand and production forecasts. These day-ahead forecasts provide hourly figures of power demand and production [30]. Based on this data, the independent system operator solves the power flow (PF) or optimal power flow (OPF) problem every T minutes—typical value is 15 minutes or so—to aid the primary, secondary and tertiary controls [31]. Each solution obtained from solving the PF/OPF corresponds to a particular operating point (also known as *equilibrium*). To describe how the proposed LRFC is implemented, consider an ideal case when the actual demand and power production by the renewables, denoted by $\boldsymbol{q}(t)$, are known and static over a short time period kT where $k \geq 0$ indicates the discrete-time index—let $\boldsymbol{q}^k$ be the predicted demand and renewable generation such that $\boldsymbol{q}(t) = \boldsymbol{q}^k$ where $kT \leq t \leq (k+1)T$. As such, the system rests at an equilibrium

with $(\boldsymbol{x}_d^k, \boldsymbol{x}_a^k)$ denoting the steady-state dynamic and algebraic states while $\boldsymbol{u}_{\text{ref}}^k$ denoting the steady-state generators' inputs.

Since the power supply and demand are balanced, then we have $\omega_i = 2\pi 60$ rad/sec for all $i \in \mathcal{G}$. Yet, in reality, the values of $\boldsymbol{q}(t)$ are highly stochastic and rapidly changing over time. In order to maintain the system's frequency as close to 60 Hz as possible, when $\boldsymbol{q}(t) \neq \boldsymbol{q}^k$ due to demand and renewables variability, the new $\boldsymbol{u}_{\text{ref}}^k$ has to be computed and this must be followed by solving the PF/OPF. This practice is impractical since $\boldsymbol{q}(t) \neq \boldsymbol{q}^k$ might happen during $kT \leq t \leq (k+1)T$ and especially when the deviations are relatively small. As a means to sustain the system's frequency at 60 Hz while still being able to solve the PF/OPF within the 15 minutes interval, we propose a state feedback control architecture in which controller gain matrix is independent from the solution of the PF/OPF. The power network's dynamics with such controller are written as

$$\dot{\boldsymbol{x}}_d = \boldsymbol{A}_d \boldsymbol{x}_d + \boldsymbol{G}_d \boldsymbol{f}_d(\boldsymbol{x}_d, \boldsymbol{x}_a) + \boldsymbol{B}_d \boldsymbol{u}_{\text{LRFC}} + \boldsymbol{h}\omega_0 \tag{5a}$$

$$\boldsymbol{0} = \boldsymbol{A}_a \boldsymbol{x}_a + \boldsymbol{G}_a \boldsymbol{f}_a(\boldsymbol{x}_d, \boldsymbol{x}_a) + \boldsymbol{B}_a \boldsymbol{q}, \tag{5b}$$

where the control input during $kT \leq t \leq (k+1)T$ is given as

$$\boxed{\boldsymbol{u}_{\text{LRFC}} := \boldsymbol{u}_{\text{LRFC}}(t) = \boldsymbol{u}_{\text{ref}}^k + \boldsymbol{K}_d\left(\boldsymbol{x}_d(t) - \boldsymbol{x}_d^k\right),}$$

in which $\boldsymbol{K}_d \in \mathbb{R}^{n_u \times n_d}$ denotes the associated controller gain matrix. In this approach, $\boldsymbol{K}_d$ is computed based only on the knowledge of matrices and functions provided in (5) and thus independent from $\boldsymbol{u}_{\text{ref}}^k$ and $(\boldsymbol{x}_d^k, \boldsymbol{x}_a^k)$. The overall structure of the proposed LRFC is depicted in Fig. 1. This control architecture only *(i)* requires the knowledge of generators' internal states—thus does not rely on any real-time measurements of algebraic variables $(\boldsymbol{a}, \tilde{\boldsymbol{v}})$ whatsoever—while *(ii)* not involving any kind of system's linearization around $(\boldsymbol{x}_d^k, \boldsymbol{x}_a^k)$. It is worth noting that the control architecture depicted in Fig. 1 is common in power systems secondary control [6], [13], [15], [19]. Now, suppose that a disturbance—attributed by a sudden change in power demands and/or power produced by the renewables—is applied to the network. This disturbance will eventually throw the system's operating point to a new equilibrium. Let us denote $\boldsymbol{q}^e$ as the new actual demand and generated power from the renewables at $kT \leq t \leq (k+1)T$ time instance. Using the proposed LRFC framework described in (5), the system's dynamics at the new steady-state operating point indicated by $(\boldsymbol{x}_d^e, \boldsymbol{x}_a^e)$ can be expressed as

$$\begin{aligned}\boldsymbol{0} = {} & \boldsymbol{A}_d \boldsymbol{x}_d^e + \boldsymbol{G}_d \boldsymbol{f}_d(\boldsymbol{x}_d^e, \boldsymbol{x}_a^e) + \boldsymbol{h}\omega_0 \\ & + \boldsymbol{B}_d\left(\boldsymbol{u}_{\text{ref}}^k + \boldsymbol{K}_d\left(\boldsymbol{x}_d^e - \boldsymbol{x}_d^k\right)\right)\end{aligned} \tag{6a}$$

$$\boldsymbol{0} = \boldsymbol{A}_a \boldsymbol{x}_a^e + \boldsymbol{G}_a \boldsymbol{f}_a(\boldsymbol{x}_d^e, \boldsymbol{x}_a^e) + \boldsymbol{B}_a \boldsymbol{q}^e, \tag{6b}$$

In order to analyze the network's dynamical behavior after the disturbance is initiated, let us introduce $\Delta\boldsymbol{x}_d \in \mathbb{R}^{n_d}$ and $\Delta\boldsymbol{x}_a \in \mathbb{R}^{n_a}$ as the *deviations* of the dynamic and algebraic states of the perturbed system around $(\boldsymbol{x}_d^e, \boldsymbol{x}_a^e)$, respectively, and they are given as $\Delta\boldsymbol{x}_d := \boldsymbol{x}_d - \boldsymbol{x}_d^e$ and $\Delta\boldsymbol{x}_a := \boldsymbol{x}_a - \boldsymbol{x}_a^e$. From (5), (6), and letting $\Delta\boldsymbol{q} := \boldsymbol{q} - \boldsymbol{q}^e$, the perturbed network's dynamics can be derived as

$$\boxed{\begin{aligned}\Delta\dot{\boldsymbol{x}}_d &= (\boldsymbol{A}_d + \boldsymbol{B}_d\boldsymbol{K}_d)\Delta\boldsymbol{x}_d + \boldsymbol{G}_d\Delta\boldsymbol{f}_d(\Delta\boldsymbol{x}_d, \Delta\boldsymbol{x}_a) && (7a)\\ \boldsymbol{0} &= \boldsymbol{A}_a\Delta\boldsymbol{x}_a + \boldsymbol{G}_a\Delta\boldsymbol{f}_a(\Delta\boldsymbol{x}_d, \Delta\boldsymbol{x}_a) + \boldsymbol{B}_a\Delta\boldsymbol{q}, && (7b)\end{aligned}}$$

where the mappings $\Delta\boldsymbol{f}_d(\cdot)$ and $\Delta\boldsymbol{f}_a(\cdot)$ are detailed as

$$\Delta\boldsymbol{f}_d(\Delta\boldsymbol{x}_d, \Delta\boldsymbol{x}_a) := \boldsymbol{f}_d(\boldsymbol{x}_d, \boldsymbol{x}_a) - \boldsymbol{f}_d(\boldsymbol{x}_d^e, \boldsymbol{x}_a^e)$$

$$\Delta\boldsymbol{f}_a(\Delta\boldsymbol{x}_d, \Delta\boldsymbol{x}_a) := \boldsymbol{f}_a(\boldsymbol{x}_d, \boldsymbol{x}_a) - \boldsymbol{f}_a(\boldsymbol{x}_d^e, \boldsymbol{x}_a^e).$$

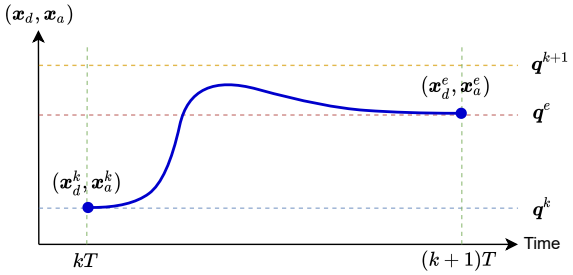

Figure 2. The LRFC is intended to stabilize the system—the actual state during $kT \leq t \leq (k+1)T$ is represented by the blue curve—when the actual power demand and renewable generation are transiting from the projected $\boldsymbol{q}^k$ at time kT to the new level $\boldsymbol{q}^e$ until $(k+1)T$.

In (7), $\Delta\boldsymbol{q}$ reflects the deviation of the current demand and renewables generation $\boldsymbol{q}$ from the new operating values $\boldsymbol{q}^e$ and as such, $\Delta\boldsymbol{q}$ is considered to be relatively small and its values are closed to zero. Our objective herein is to design the gain matrix $\boldsymbol{K}_d$ such that all trajectories of the solutions of the NDAE (7) will converge asymptotically towards the zero equilibrium with respect to the disturbance caused by $\Delta\boldsymbol{q}$. This is equivalent for the states of power network (6) to converge towards the new operating point indicated by $(\boldsymbol{x}_d^e, \boldsymbol{x}_a^e)$. This process is illustrated in Fig. 2. The following section focuses on the design of stabilizing $\boldsymbol{K}_d$ posed as a convex semi-definite programming (SDP) problem.

B. Stabilization of Power Network's NDAEs

To simplify the notations, let $\boldsymbol{x}_d := \Delta\boldsymbol{x}_d$, $\boldsymbol{x}_a := \Delta\boldsymbol{x}_a$, $\boldsymbol{f}_d := \Delta\boldsymbol{f}_d$, and $\boldsymbol{f}_a := \Delta\boldsymbol{f}_a$ such that (7) can be written as

$$\boldsymbol{E}_d\dot{\boldsymbol{x}}_d = (\boldsymbol{A}_d + \boldsymbol{B}_d\boldsymbol{K}_d)\boldsymbol{x}_d + \boldsymbol{G}_d\boldsymbol{f}_d(\boldsymbol{x}_d, \boldsymbol{x}_a) \tag{8a}$$

$$\boldsymbol{0} = \boldsymbol{A}_a\boldsymbol{x}_a + \boldsymbol{G}_a\boldsymbol{f}_a(\boldsymbol{x}_d, \boldsymbol{x}_a), \tag{8b}$$

where $\boldsymbol{E}_d = \boldsymbol{I}$ for the power network model described in (7)*. Albeit the NDAE (8) assumes that $\Delta\boldsymbol{q} = \boldsymbol{0}$, in Section IV we study the performance of the LRFC when disturbance is present and therefore, the stability of (7) is analyzed against a nonzero disturbance. It is also assumed herein that $\boldsymbol{x}_d \in \boldsymbol{\mathcal{X}}_d \subseteq \mathbb{R}^{n_d}$ and $\boldsymbol{x}_a \in \boldsymbol{\mathcal{X}}_a \subseteq \mathbb{R}^{n_a}$. That is, the sets $\boldsymbol{\mathcal{X}}_d$ and $\boldsymbol{\mathcal{X}}_a$ represent the operating region(s) of the power networks and contain the solution manifold of (8). The following assumptions (which are standard in the literature on control and stabilization of DAEs [27], [28]) are crucial for the development of our LRFC method and therefore considered throughout the paper.

Assumption 1. *The following properties hold for the mappings $\boldsymbol{f}_d : \mathbb{R}^{n_d} \times \mathbb{R}^{n_a} \to \mathbb{R}^{n_{fd}}$ and $\boldsymbol{f}_a : \mathbb{R}^{n_d} \times \mathbb{R}^{n_a} \to \mathbb{R}^{n_{fa}}$:*

1) $\boldsymbol{f}_d(\cdot)$ and $\boldsymbol{f}_a(\cdot)$ are smooth and satisfy $\boldsymbol{f}_d(\boldsymbol{0}, \boldsymbol{0}) = \boldsymbol{0}$ and $\boldsymbol{f}_a(\boldsymbol{0}, \boldsymbol{0}) = \boldsymbol{0}$.

2) $\boldsymbol{f}_d(\cdot)$ and $\boldsymbol{f}_a(\cdot)$ are quadratically-bounded functions such that, given $\boldsymbol{x}_d \in \boldsymbol{\mathcal{X}}_d$ and $\boldsymbol{x}_a \in \boldsymbol{\mathcal{X}}_a$, it holds that

$$\|\boldsymbol{f}_d(\boldsymbol{x}_d, \boldsymbol{x}_a)\|_2^2 \leq \left\|\boldsymbol{H}_d^d\boldsymbol{x}_d(t)\right\|_2^2 + \left\|\boldsymbol{H}_a^d\boldsymbol{x}_a(t)\right\|_2^2 \tag{9a}$$

$$\|\boldsymbol{f}_a(\boldsymbol{x}_d, \boldsymbol{x}_a)\|_2^2 \leq \|\boldsymbol{H}_d^a\boldsymbol{x}_d(t)\|_2^2 + \|\boldsymbol{H}_a^a\boldsymbol{x}_a(t)\|_2^2, \tag{9b}$$

for some known constant matrices $\boldsymbol{H}_d^d$, $\boldsymbol{H}_a^d$, $\boldsymbol{H}_d^a$, $\boldsymbol{H}_a^a$.

*The matrix $\boldsymbol{E}_d$ is kept in the controller derivations for the sake of generality since, albeit we do have $\boldsymbol{E}_d = \boldsymbol{I}$ in (7), the state-space representation of power networks (1)-(3) is *not* unique and thus, it is possible to have $\boldsymbol{E}_d \neq \boldsymbol{I}$.

Assumption 2. *This rank equality*

$$\operatorname{rank}\left(\boldsymbol{A}_a+\boldsymbol{G}_a\frac{\partial \boldsymbol{f}_a\left(\boldsymbol{x}_d,\boldsymbol{x}_a\right)}{\partial \boldsymbol{x}_a}\right)=n_a, \tag{10}$$

is satisfied for all $\boldsymbol{x}_d \in \boldsymbol{\mathcal{X}}_d$ and $\boldsymbol{x}_a \in \boldsymbol{\mathcal{X}}_a$.

It is worth mentioning that Assumption 1 is mild in power networks—see [6], [15], [19]. In fact, it is shown in [15] that, for a simplified ODE representation of power networks with turbine governor dynamics, there exist bounding matrices such that (9a) holds without the presence of $\boldsymbol{x}_a$. In principle, the nonlinearities in the NDAE model are treated as external disturbances originated from the network's interconnections and as such, since their influence towards the system is bounded according to (9), the designed stabilizing controller attempts to compensate impacts caused by these disturbances.

In DAE systems theory, differentiation index can be associated with the minimum number of steps required for expressing the corresponding DAE in an explicit form [22], [32]. The condition (10) is useful to ensure that the NDAE (8) is of index one [28]. For a simplified model of multi-machine power networks, it is proved in [22] that power networks' DAEs are of index one if every load bus is connected to at least one generator bus. Since this is the case in normal conditions (e.g., no tripping in power lines), then Assumption 2 is easily satisfied. Although the property introduced in [22] is studied for a simplified model without involving any renewables, it is revealed that the condition (10) actually holds for a more comprehensive model of power networks considered in this paper—this is evident from being able to numerically simulate power networks for various test cases (see Section IV). Hence, based on the above assumptions, we now focus on providing a computational approach to calculate the state feedback gain matrix $\boldsymbol{K}_d$ such that the NDAE (8) is asymptotically stable. That is, the NDAE (8) is said to be asymptotically stable if $\lim_{t\to\infty}\|\boldsymbol{x}_d(t)\|_2=0$ and $\lim_{t\to\infty}\|\boldsymbol{x}_a(t)\|_2=0$ [33]. The following result provides a sufficient condition for the asymptotic stability of NDAE (8) at the origin.

Theorem 1. *Consider the NDAE (8) provided that Assumptions 1 and 2 hold. The closed-loop system is asymptotically stable around the origin if there exist matrices $\boldsymbol{Q}_1 \in \mathbb{R}^{n_d\times n_d}$, $\boldsymbol{Q}_2 \in \mathbb{R}^{n_a\times n_d}$, $\boldsymbol{Q}_3 \in \mathbb{R}^{n_a\times n_a}$, where both $\boldsymbol{Q}_1$ and $\boldsymbol{Q}_3$ are nonsingular, and a scalar $\bar{\epsilon} \in \mathbb{R}_{++}$ such that the following nonconvex matrix inequality is feasible*

$$\begin{bmatrix} \boldsymbol{\Upsilon} & * & * & * \\ \boldsymbol{A}_a\boldsymbol{Q}_2 & \boldsymbol{Q}_3^\top\boldsymbol{A}_a^\top+\boldsymbol{A}_a\boldsymbol{Q}_3+\bar{\epsilon}\boldsymbol{G}_a\boldsymbol{G}_a^\top & * & * \\ \bar{\boldsymbol{H}}_d^{\frac{1}{2}}\boldsymbol{Q}_1 & \boldsymbol{O} & -\bar{\epsilon}\boldsymbol{I} & * \\ \bar{\boldsymbol{H}}_a^{\frac{1}{2}}\boldsymbol{Q}_2 & \bar{\boldsymbol{H}}_d^{\frac{1}{2}}\boldsymbol{Q}_3 & \boldsymbol{O} & -\bar{\epsilon}\boldsymbol{I} \end{bmatrix} \prec 0 \tag{11a}$$

$$\boldsymbol{E}_d^\top\boldsymbol{Q}_1^{-1}=\boldsymbol{Q}_1^{-\top}\boldsymbol{E}_d \succ 0 \tag{11b}$$

where $\boldsymbol{\Upsilon}$ includes the matrix $\boldsymbol{K}_d$ and is defined as

$$\boldsymbol{Q}_1^\top\boldsymbol{A}_d^\top+\boldsymbol{A}_d\boldsymbol{Q}_1+\boldsymbol{Q}_1^\top\boldsymbol{K}_d^\top\boldsymbol{B}_d^\top+\boldsymbol{B}_d\boldsymbol{K}_d\boldsymbol{Q}_1+\bar{\epsilon}\boldsymbol{G}_d\boldsymbol{G}_d^\top,$$

The matrices $\bar{\boldsymbol{H}}_d$ and $\bar{\boldsymbol{H}}_a$ in (11a) are specified as

$$\bar{\boldsymbol{H}}_d:=\boldsymbol{H}_d^{d\top}\boldsymbol{H}_d^d+\boldsymbol{H}_d^{a\top}\boldsymbol{H}_d^a,\quad \bar{\boldsymbol{H}}_a:=\boldsymbol{H}_a^{d\top}\boldsymbol{H}_a^d+\boldsymbol{H}_a^{a\top}\boldsymbol{H}_a^a.$$

The complete proof of Theorem 1 is available in Appendix B. The satisfaction of matrix inequalities (11) guarantees the existence of $\boldsymbol{K}_d$ that asymptotically stabilizes the NDAE (8) around the zero equilibrium. Realize that, since the states of the NDAE (8) in fact are just the deviations of the actual states $(\boldsymbol{x}_d,\boldsymbol{x}_a)$ from the new operating point $(\boldsymbol{x}_d^e,\boldsymbol{x}_a^e)$, then it can be easily deduced that

$$\lim_{t\to\infty}\Delta\boldsymbol{x}_d(t)=0 \;\Rightarrow\; \lim_{t\to\infty}\boldsymbol{x}_d(t)=\boldsymbol{x}_d^e$$
$$\lim_{t\to\infty}\Delta\boldsymbol{x}_a(t)=0 \;\Rightarrow\; \lim_{t\to\infty}\boldsymbol{x}_a(t)=\boldsymbol{x}_a^e.$$

Since $\boldsymbol{x}_d^e$ consists of the synchronous frequency for the rotors of all rotating machines, then we have $\omega_i=2\pi 60$ rad/sec for all $i\in\mathcal{G}$. In short, the proposed state feedback control strategy with gain matrix $\boldsymbol{K}_d$ is able to provide LRFC due to the changes in power demands and renewables generation. Unfortunately, the majority off-the-shelf optimization packages, such as CVX [34] and YALMIP [35], cannot be utilized to find solutions for (11) due to the nonconvexity of the problem, which is partly attributed to the appearance of $\boldsymbol{Q}_1^{-1}$ in (11b) along with the existence of bilinear term $\boldsymbol{K}_d\boldsymbol{Q}_1$. To circumvent this design challenge, the following result is proposed.

Proposition 1. *Consider the NDAE (8) given that Assumptions 1 and 2 hold. The closed-loop system is asymptotically stable around the origin if there are matrices $\boldsymbol{X}_1 \in \mathbb{S}_{++}^{n_d}$, $\boldsymbol{X}_2 \in \mathbb{R}^{n_a\times n_d}$, $\boldsymbol{R} \in \mathbb{R}^{n_a\times n_a}$, $\boldsymbol{Y} \in \mathbb{R}^{n_d\times n_a}$, $\boldsymbol{W} \in \mathbb{R}^{n_u\times n_d}$, and a scalar $\bar{\epsilon} \in \mathbb{R}_{++}$ such that the following LMI is feasible*

$$\begin{bmatrix} \boldsymbol{\Psi} & * & * & * \\ \boldsymbol{A}_a\boldsymbol{X}_2\boldsymbol{E}_d^\top+\boldsymbol{A}_a\boldsymbol{Y} & \boldsymbol{\Theta} & * & * \\ \bar{\boldsymbol{H}}_d^{\frac{1}{2}}\boldsymbol{X}_1\boldsymbol{E}_d^\top & \boldsymbol{O} & -\bar{\epsilon}\boldsymbol{I} & * \\ \bar{\boldsymbol{H}}_a^{\frac{1}{2}}\boldsymbol{X}_2\boldsymbol{E}_d^\top+\bar{\boldsymbol{H}}_a^{\frac{1}{2}}\boldsymbol{Y} & \bar{\boldsymbol{H}}_d^{\frac{1}{2}}\boldsymbol{R} & \boldsymbol{O} & -\bar{\epsilon}\boldsymbol{I} \end{bmatrix} \prec 0, \tag{12}$$

where $\boldsymbol{\Psi}$ is specified as

$$\boldsymbol{E}_d\boldsymbol{X}_1\boldsymbol{A}_d^\top+\boldsymbol{A}_d\boldsymbol{X}_1\boldsymbol{E}_d^\top+\boldsymbol{E}_d\boldsymbol{W}^\top\boldsymbol{B}_d^\top+\boldsymbol{B}_d\boldsymbol{W}\boldsymbol{E}_d^\top+\bar{\epsilon}\boldsymbol{G}_d\boldsymbol{G}_d^\top,$$

and $\boldsymbol{\Theta}:=\boldsymbol{R}^\top\boldsymbol{A}_a^\top+\boldsymbol{A}_a\boldsymbol{R}+\bar{\epsilon}\boldsymbol{G}_a\boldsymbol{G}_a^\top$. Upon solving (12), the controller gain $\boldsymbol{K}_d$ can be recovered as $\boldsymbol{K}_d=\boldsymbol{W}\boldsymbol{X}_1^{-1}$.

Readers are referred to Appendix C for the proof of Proposition 1. In contrast to matrix inequality (11), the one given in (12) constitutes an LMI and therefore can be easily solved through standard convex optimization packages.

For practical reason, it is often desired to obtain small feedback gains so that the resulting transient behaviors can be kept within acceptable bounds and do not strain the system protection [6]. Moreover, a high gain controller is in general undesirable since it can increase the sensitivity of the closed-loop system against noise and uncertainty. To that end, we consider solving the following optimization problem in the interest of obtaining $\boldsymbol{K}_d$ with a reasonable magnitude.

$$(\mathbf{P}) \quad \underset{\bar{\epsilon},\boldsymbol{X}_1,\boldsymbol{X}_2,\boldsymbol{R},\boldsymbol{Y},\boldsymbol{W}}{\text{minimize}} \quad \kappa\|\boldsymbol{W}\|_2$$
$$\text{subject to} \quad (12),\ \boldsymbol{X}_1\succ 0,\ \bar{\epsilon}>0,$$

where $\kappa\in\mathbb{R}_{++}$ is a predefined constant and $\|\boldsymbol{W}\|_2$ denotes the induced 2-norm of matrix $\boldsymbol{W}$.

C. Implementation of The Proposed LRFC Strategy

The proposed LRFC strategy can be implemented as follows. First, based on the matrices describing the network dynamics (4), the controller gain $\boldsymbol{K}_d$ is computed by solving problem $\mathbf{P}$. Based on the load and renewable forecasts $\boldsymbol{q}^k$, the steady-state algebraic variables $\boldsymbol{x}_a^k$ can be obtained from solving the PF/OPF. Afterwards, $(\boldsymbol{x}_d^k,\boldsymbol{u}_{\text{ref}}^k)$ can be computed by setting $\dot{\boldsymbol{x}}_d=0$ in (4)

Algorithm 1: Implementation of The LRFC

input: $\boldsymbol{A}_d$, $\boldsymbol{A}_a$, $\boldsymbol{G}_d$, $\boldsymbol{G}_a$, $\boldsymbol{B}_d$, $\boldsymbol{B}_a$, T
compute: $\boldsymbol{K}_d$ by solving problem $\mathbf{P}$
initialize: iteration index $k = 0$
do
  obtain: $\boldsymbol{q}^k$ from prediction and measurement
  solve: PF/OPF based on $\boldsymbol{q}^k$
  get: $\boldsymbol{x}_a^k$ from the solution of PF/OPF
  compute: $\boldsymbol{u}_{\text{ref}}^k$ and $\boldsymbol{x}_d^k$
  update: the LRFC in Fig. 1 with $(\boldsymbol{x}_d^k, \boldsymbol{u}_{\text{ref}}^k)$
  wait: T minutes // ***OPF Time-Period***
  update: $k \leftarrow k + 1$
while $k < \infty$

and from $(\boldsymbol{q}^k, \boldsymbol{x}_a^k)$, the resulting system of nonlinear equations is numerically solved. The calculated $(\boldsymbol{x}_d^k, \boldsymbol{u}_{\text{ref}}^k)$ is then fed to the control architecture illustrated in Fig. 1. These steps are then repeated once every T, which is typically around 15 minutes [31], to continuously perform LRFC and compensate any changes in demand and renewables generation. Algorithm 1 presents a summary on how the LRFC is implemented. Realize that, since the matrix $\boldsymbol{K}_d$ is only computed *once*, our approach for LRFC is much more practical compared to other methods that rely on the linearization of (4) around the operating point $(\boldsymbol{x}_d^k, \boldsymbol{x}_a^k)$ because, in addition to solving the PF/OPF and the set of nonlinear equations mentioned above, the independent system operator has to *(a)* perform the linearization while also *(b)* computing the stabilizing controller gain matrix—two are carried out in each iteration within $kT \leq t \leq (k+1)T$ time interval. This linearization-based approach certainly necessitates more demanding computational processes to be performed.

IV. Numerical Case Studies

A. Parameters and Setup for Numerical Simulation

This section presents numerical simulations for investigating the performance of the proposed approach in stabilizing several IEEE test networks with respect to load and renewable disturbances. Every numerical simulation is performed using MATLAB R2020b running on a 64-bit Windows 10 with a 3.0GHz AMD Ryzen™ 9 4900HS processor and 16 GB of RAM, whereas all convex SDPs are solved through YALMIP [35] optimization interface along with MOSEK [36] solver. All dynamical simulations for NDAEs are performed using MATLAB's index-one DAEs solver `ode15i`. Four power networks are considered in this study:

- 9-*bus network*: The Western System Coordinating Council (WSCC) 9-bus system with 3 synchronous generators.
- 14-*bus network*: Consisting of 14-bus system with 5 synchronous generators, representing a portion of the American Electric Power System (AEPS) in the Midwestern US.
- 39-*bus network*: Represents the New England 10-machine, 39-bus system.
- 57-*bus network*: Consisting of 57 buses with 7 synchronous generators, which again represents a part of the AEPS.

In this study the loads are presumed to be of constant power type while renewable power plants—such as wind farms and solar PVs—are modeled as loads with *negative* power, thereby injecting active power to the network. For the 9-bus and 14-bus networks, every load bus is connected to one renewable power plant. For the 39-bus and 57-bus networks, one renewable power plant is attached to a load bus when the consumed power is equal or exceeds $3\,\text{pu}$ and $0.1\,\text{pu}$, respectively. The initial conditions as well as steady-state values of the power network before disturbance is applied are computed from the solutions of power flow, which is obtained from MATPOWER [37] function `runpf`. The power base for all power system cases is chosen to be 100 MVA. The synchronous generator parameters are obtained from Power System Toolbox (PST) [29]. Since the regulation and chest time constants are not specified in PST, their values are chosen to be $R_{\text{D}i} = 0.02$ Hz/pu and $T_{\text{CH}i} = 0.2$ sec, respectively, for all generators [13].

Table II
THE COMPARISON OF THE TOTAL ROTOR SPEED DEVIATIONS WITH RESPECT TO DIFFERENT LEVELS OF DISTURBANCE TAKEN AT $t = 15$ SEC, EXCEPT FOR THE 9-BUS NETWORK WHERE $t = 10$ SEC DUE TO SLOW CONVERGENCE AS SEEN FROM FIG. 3. THE DASH SYMBOL "–" INDICATES THAT THE ROTOR SPEED DOES NOT CONVERGE AND BOLD NUMBERS INDICATE THE MINIMUM VALUES.

Network	$\rho_{\text{L}} = -\rho_{\text{R}}$	$\left(\left\|\omega_0 \times \mathbf{1} - \boldsymbol{\omega}(\tilde{t}_k)\right\|_2 \times 10^3\right)$		
		NDAE-control	LQR-control	AGC
9-bus	0.04	**0.177**	1.656	1.575
	0.08	**0.354**	3.538	–
	0.12	**0.543**	–	–
14-bus	0.04	$\mathbf{6.437 \times 10^{-7}}$	3.046	3.406
	0.08	$\mathbf{9.409 \times 10^{-6}}$	6.152	–
	0.12	$\mathbf{4.433 \times 10^{-6}}$	–	–
39-bus	0.01	$\mathbf{2.027 \times 10^{-5}}$	10.820	–
	0.05	$\mathbf{5.130 \times 10^{-6}}$	–	–
57-bus	0.005	$\mathbf{8.092 \times 10^{-6}}$	1.534	–
	0.01	$\mathbf{1.592 \times 10^{-5}}$	–	–

B. LRFC Under Different Levels of Step Disturbance

Herein, we analyze the performance of the proposed control strategy—which is referred to as *NDAE-control*—in performing LRFC for the aforementioned power network test cases against two control strategies prominent in power systems literature, namely the Automatic Generation Control (AGC) and Linear Quadratic Regulator (LQR) control (referred to as *LQR-control*). We do not compare our method with the ones proposed in [6], [15], [16], [19] since these methods are designed for the simplified nonlinear ODE model of power networks, and thus are not applicable for performing LRFC using the model given in (4). The controller gain for the NDAE-control is obtained from solving problem $\mathbf{P}$ with $\kappa = 10^{-3}$. Since the form of nonlinearities in $\boldsymbol{f}_d(\cdot)$ and $\boldsymbol{f}_a(\cdot)$ are much more complex than the ones in [6], [15], [19], the associated bounding matrices for both of these mappings are instead set to be

$$\left(\boldsymbol{H}_d^d\right)^2 = \boldsymbol{I},\ \left(\boldsymbol{H}_a^d\right)^2 = \boldsymbol{I},\ \left(\boldsymbol{H}_d^a\right)^2 = \boldsymbol{I},\ \left(\boldsymbol{H}_a^a\right)^2 = \boldsymbol{I},$$

for the 9-bus and 14-bus networks while the following values

$$\left(\boldsymbol{H}_d^d\right)^2 = 10\boldsymbol{I},\ \left(\boldsymbol{H}_a^d\right)^2 = 10\boldsymbol{I},\ \left(\boldsymbol{H}_d^a\right)^2 = 10\boldsymbol{I},\ \left(\boldsymbol{H}_a^a\right)^2 = 10\boldsymbol{I},$$

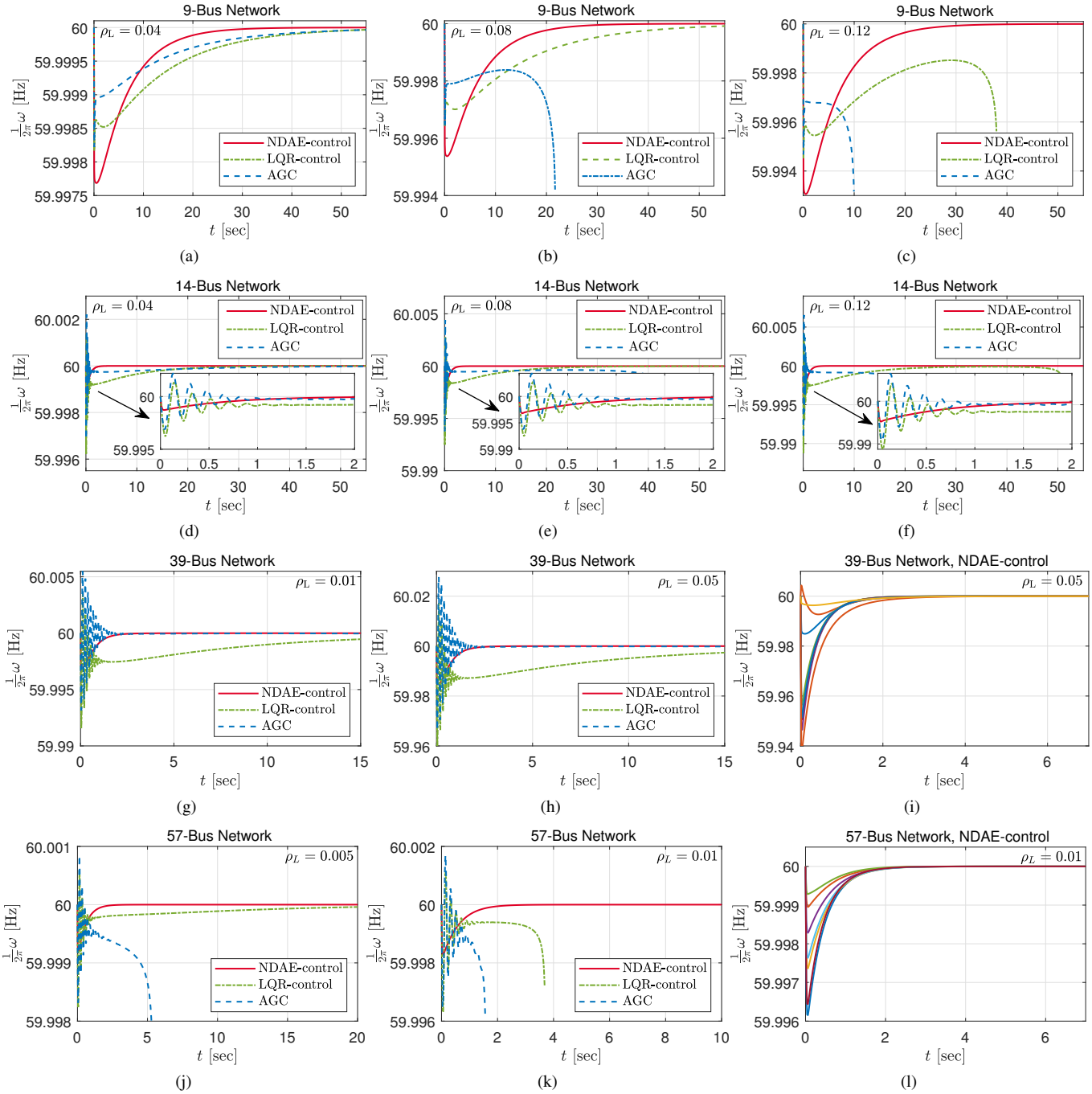

Figure 3. Numerical simulation results: Figs. (a), (b), (c) illustrate the frequency of Generator 1 for the 9-bus network; Figs. (d), (e), (f) illustrate the frequency of Generator 1 for the 14-bus network; Figs. (g) and (h) illustrate the frequency of Generator 1 while Fig. (i) shows all generators' frequency for the 39-bus network with the NDAE-control; Figs. (j) and (k) illustrate the frequency of Generator 1 while Fig. (l) shows all generators' frequency for the 57-bus network with the NDAE-control. Although the trajectories of the rotor frequency for the 39-bus network given in Figs. (g) and (h) seem to converge, the AGC actually fails to stabilize the system for $\rho_L = 0.01$ and $\rho_L = 0.05$ while the LQR-control cannot stabilize the system when $\rho_L = 0.05$.

are selected for the 39-bus and 57-bus networks. The bounding matrices for the 39-bus and 57-bus networks are set to be larger than those for the 9-bus and 14-bus networks since the 39-bus and 57-bus networks are comprised of significantly larger nodes and interconnections. For the AGC, it is implemented based on the method described in [13], [38], where it provides a set of control inputs for the governor reference signals only. The AGC calculates such input signals from adding an extra dynamic state χ to the power network model (4), specified as

$$\dot{\chi} = K_{\rm G}\left(-\chi - {\rm ACE} + \sum_{i=1}^{G}(P_{{\rm G}i} - P_{{\rm G}i}^0)\right), \qquad (13)$$

where $K_{\rm G}$ is an integrator gain for the AGC dynamics, which value is set to be 1000, and $P_{{\rm G}i}^0$ is the i-th steady-state generator active power before disturbance. The term ACE in (13) stands for *area control error* and defined as [13]

$${\rm ACE} := \frac{1}{G}\sum_{i=1}^{G}(\frac{1}{R_{{\rm D}i}} + D_i)(\omega_i - \omega_0).$$

Following [39], each power network is treated as a single area. The governor reference signal for each generator $i \in \mathcal{G}$ is given as $T_{{\rm CH}i} = T_{{\rm CH}i}^0 + K_i\chi$, where $K_i := P_{{\rm G}i}/\sum_{i=1}^{G} P_{{\rm G}i}$, for every $i \in \mathcal{G}$, indicates the participation factor of each generator such that $\sum_{i=1}^{G} K_i = 1$, and $T_{{\rm CH}i}^0$ is the corresponding steady-state governor reference signal before disturbance. However, since AGC only provides value for $T_{{\rm CH}i}$, the control inputs for the internal field voltage are calculated with the aid from LQR-control. It is important to mention that the controller gain for LQR-control is retrieved from solving the corresponding LMI specified in Theorem 1 of [40], which is reliant on the *linearized* dynamics corresponding to the initial operating point.

The numerical simulation is performed as follows. Initially, the system operates with total load of $\left(P_{\rm L}^0, Q_{\rm L}^0\right)$ and total generated power from renewables of $\left(P_{\rm R}^0, Q_{\rm R}^0\right)$. For each of the power network test cases, the following values are chosen: $P_{\rm L}^0 + jQ_{\rm L}^0 = 3.15 + j1.15$ pu and $P_{\rm R}^0 + jQ_{\rm R}^0 = 0.63$ pu for the 9-bus network, $P_{\rm L}^0 + jQ_{\rm L}^0 = 3.15 + j1.15$ pu and $P_{\rm R}^0 + jQ_{\rm R}^0 = 0.63$ pu for the 14-bus network, $P_{\rm L}^0 + jQ_{\rm L}^0 = 62.5423 + j13.871$ pu and $P_{\rm R}^0 + jQ_{\rm R}^0 = 8.1712$ pu for the 39-bus network, while $P_{\rm L}^0 + jQ_{\rm L}^0 = 12.508 + j3.364$ pu and $P_{\rm R}^0 + jQ_{\rm R}^0 = 2.2888$ pu for the 57-bus network. Immediately after $t > 0$, the loads and renewables are experiencing an abrupt step change in the amount of consumed and produced power, which triggers the system to depart from its initial equilibrium point. The new value of complex power for loads and renewables are specified as $P_{\rm L}^e + jQ_{\rm L}^e := (1 + \rho_{\rm L})(P_{\rm L}^0 + jQ_{\rm L}^0)$ and $P_{\rm R}^e + jQ_{\rm R}^e := (1 + \rho_{\rm R})(P_{\rm R}^0 + jQ_{\rm R}^0)$ where $\rho \in \mathbb{R}$ determines the quantity of the disturbance. In this numerical simulation, we consider different levels of disturbance: $\rho_{\rm L} = 0.04$, $\rho_{\rm L} = 0.08$, and $\rho_{\rm L} = 0.12$ for the 9-bus network and 14-bus network, $\rho_{\rm L} = 0.01$, and $\rho_{\rm L} = 0.05$ for the 39-bus network, and $\rho_{\rm L} = 0.005$ and $\rho_{\rm L} = 0.01$ for the 57-bus network. For the disturbance coming from renewables, we select $\rho_{\rm R} = -\rho_{\rm L}$.

The results of the numerical simulation are illustrated in Fig. 3. For the 9-bus network, the proposed NDAE-control is able to stabilize the system even when the disturbance is considerably high (12% for this network). This is in contrast to the AGC and LQR-control, as they are only able to maintain stability with relatively low (4%) and moderate (8%) disturbances. A similar behavior is also observed from the simulation results for the 14-bus, 39-bus, and 57-bus networks: the LQR-control is not able to maintain frequency stability when the disturbance achieves 12%, 5%, and 1% while the AGC fails even with 8%, 1%, and 0.5% disturbance, respectively, for the 14-bus, 39-bus, and 57-bus networks. It is seen from Fig. 3 that the frequency trajectories due to the NDAE-control converge rapidly to the equilibrium point ω_0, unlike the other controllers—Table II presents the norm of rotor speed deviations for all generators with respect to various levels of disturbance. It is evident that the NDAE-control can provide stabilization for the power networks with a decent convergence rate. It is also observed that each controller brings the system's operating point to a new equilibrium—this can be seen from the trajectories of active power and bus voltage for the 14-bus network with low disturbance as shown in Fig. 5.

C. Assessment Against Renewable Generation Uncertainties

In this section we study the 14-bus network while injecting the generated power from renewables with random Gaussian noise $z_i(t)$ with zero mean and variance of $0.01(P_{{\rm R}i}^0 + jQ_{{\rm R}i}^0)$ for each $i \in \mathcal{R}$ such that

$$P_{{\rm R}i}^e + jQ_{{\rm R}i}^e := (1+\rho_{\rm R})(P_{{\rm R}i}^0 + jQ_{{\rm R}i}^0) + (1+j)z_i(t), \quad \forall i \in \mathcal{R}.$$

To compensate the random noise, the simulation is performed 10 times and the resulting outcomes are averaged. The results of this numerical simulation with low step disturbance $\rho_{\rm L} = 0.04$ are illustrated in Fig. 4, from which it can be seen that the maximum and minimum frequency deviations for the NDAE-control are experiencing much mode fluctuations compared to those from the LQR-control and AGC. The NDAE-control is able to maintain generator's frequency close to 60 Hz without exhibiting significant oscillations. It is also indicated from this figure that, for the NDAE-control, the average bus voltage across the network has a roughly flat profile. This result can be attributed to the centralized control structure in the LQR-control and AGC, while the proposed DAE-control actually implements a decentralized control framework—discussed in Section IV-D.

D. On The Controller Gain's Sparsity Structure

Decentralized control is much more preferable than centralized control since in the former type of control, stabilization can be maintained using local measurements only. As such, our NDAE-control is more practical than AGC and LQR since the NDAE-control implements a decentralized control structure—this is indicated by the certain sparsity pattern on the feedback gain matrix $\boldsymbol{K}_d$. The patterns for the 9-bus and 14-bus networks are described in Fig. 6. The red circles denote entries with significant magnitudes, i.e., entries which magnitudes are greater or equal to 10^{-6}. Notice that the dynamic states are ordered as $\boldsymbol{x}_d := \left[\boldsymbol{\delta}^\top \ \boldsymbol{\omega}^\top \ \boldsymbol{E}'^\top \ \boldsymbol{T}_{\rm M}^\top\right]^\top$ according to Section II. Based on this ordering, the patterns depicted in Fig. 6 suggest that the inputs for each generator can be constructed from local measurements (or estimation) of its internal states. The decentralized control structure allows the internal field voltage

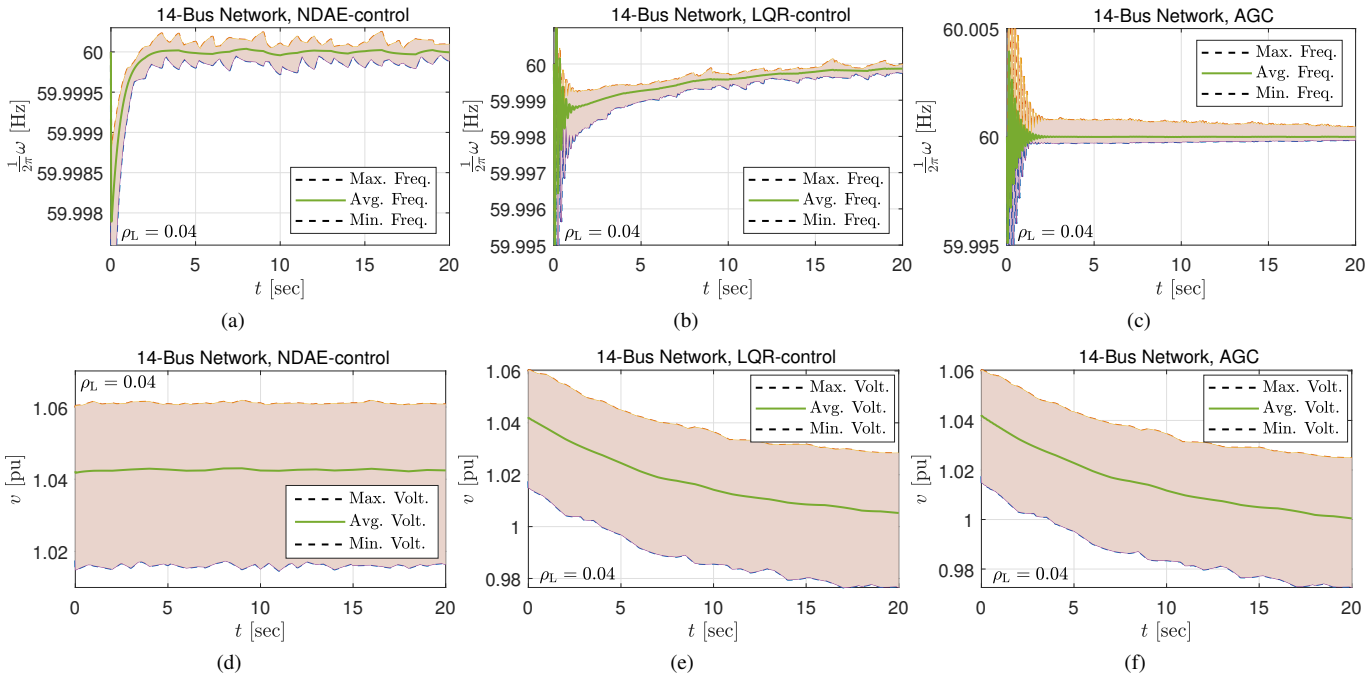

Figure 4. Numerical simulation results for the 14-bus network with renewables uncertainty: Figs. (a), (b), (c) illustrate the overall frequency figure of all generators while Figs. (d), (e), (f) illustrate the overall modulus of bus voltage for all buses using the NDAE-control, LQR-control, and AGC, respectively.

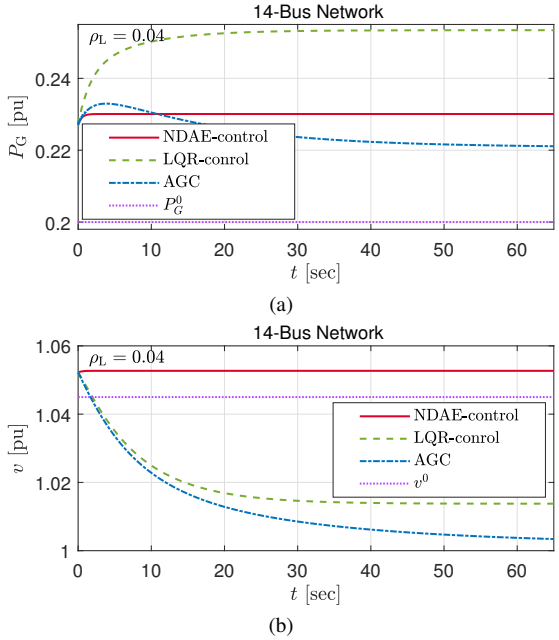

Figure 5. The trajectories of active power produced by Generator 5 (a) and the modulus of the voltage at Bus 2 (b) for the 14-bus power network with $\rho_L = 0.04$. The notations P_G^0 and v^0 represent the corresponding initial steady-state values before disturbance is applied to the network.

to be constructed by $E_{\mathrm{fd}i} = K_{D(i,2G+i)}E_i'$ while the governor reference signal to be given by

$$T_{\mathrm{r}i} = K_{D(G+i,i)}\delta_i + K_{D(G+i,G+i)}\omega_i + K_{D(G+i,3G+i)}T_{\mathrm{M}i},$$

for all $i \in \mathcal{G}$ where $K_{D(i,j)}$ is the $(i,j)-$th element of $\boldsymbol{K}_d$. The sparsity structure of $\boldsymbol{K}_d$ is suspected to be caused by the use of (8) when the matrix $\boldsymbol{K}_d$ is synthesized for the NDAE-control since the NDAE model in (8) retains the structure of the power network while, in contrast, this structure is lost in the linearized power network's model used in AGC and LQR.

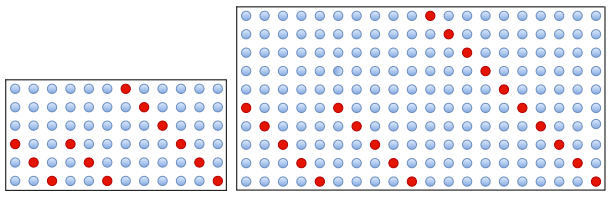

Figure 6. Sparsity pattern of the controller gain matrix $\boldsymbol{K}_d$ for the 9-bus (a) and 14-bus (b) networks. The red circles represent entries with significant magnitudes. Similar patterns are also found on the remaining larger networks.

V. Summary and Future Directions

A novel approach for LRFC in multi-machine power networks is proposed. In contrast to other methods from the literature, our approach is based on the NDAE representation of power networks and accordingly, we develop a computational approach based on LMI to construct the stabilizing controller gain matrix. The proposed approach stands out in the following manner: *(a)* its independence from any linearization around any operating points, *(b)* the resulting controller gain matrix can sufficiently maintain system's frequency around the desired equilibrium against significant disturbances originating from the loads and renewables, and *(c)* although our approach relies on advanced DAE systems theory, the proposed LRFC strategy is as simple as proportional decentralized control framework and therefore, can be implemented to large-scale power systems without the need for any special tools.

In our future work, we are planning to *(i)* extend the NDAE-control to tackle parametric uncertainties, *(ii)* investigate the theory behind the decentralized sparsity pattern of the controller gain given by the NDAE-control, and *(iii)* examine the controller's applicability to perform wide-area damping control in inverter-based, renewables-heavy power networks.

REFERENCES

[1] "U.S. energy information administration - EIA - independent statistics and analysis," accessed: 04-10-2021. [Online]. Available: https://www.eia.gov/todayinenergy/detail.php?id=46676

[2] W. Moomaw, F. Yamba, M. Kamimoto, L. Maurice, J. Nyboer, K. Urama, T. Weir, A. Jäger-Waldau, V. Krey, R. Sims, J. Steckel, M. Sterner, R. Stratton, A. Verbruggen, and R. Wiser, *Renewable Energy and Climate Change*, Jan. 2012, pp. 161–207.

[3] C. Zhao, U. Topcu, and S. H. Low, "Frequency-based load control in power systems," in *2012 American Control Conference (ACC)*, 2012, pp. 4423–4430.

[4] B. J. Kirby, "Frequency control concerns in the north american electric power system," Mar. 2003.

[5] Xiaofeng Yu and K. Tomsovic, "Application of linear matrix inequalities for load frequency control with communication delays," *IEEE Transactions on Power Systems*, vol. 19, no. 3, pp. 1508–1515, 2004.

[6] L. D. Marinovici, J. Lian, K. Kalsi, P. Du, and M. Elizondo, "Distributed hierarchical control architecture for transient dynamics improvement in power systems," *IEEE Transactions on Power Systems*, vol. 28, no. 3, pp. 3065–3074, 2013.

[7] Y. V. Hote and S. Jain, "PID controller design for load frequency control: Past, present and future challenges," *IFAC-PapersOnLine*, vol. 51, no. 4, pp. 604–609, 2018, 3rd IFAC Conference on Advances in Proportional-Integral-Derivative Control PID 2018.

[8] J. H. Chow and S. G. Ghiocel, *An Adaptive Wide-Area Power System Damping Controller using Synchrophasor Data*. New York, NY: Springer New York, 2012, pp. 327–342.

[9] A. C. Zolotas, B. Chaudhuri, I. M. Jaimoukha, and P. Korba, "A study on lqg/ltr control for damping inter-area oscillations in power systems," *IEEE Transactions on Control Systems Technology*, vol. 15, no. 1, pp. 151–160, 2007.

[10] A. Jain, E. Biyik, and A. Chakrabortty, "A model predictive control design for selective modal damping in power systems," in *2015 American Control Conference (ACC)*, 2015, pp. 4314–4319.

[11] F. Dörfler, M. R. Jovanović, M. Chertkov, and F. Bullo, "Sparsity-promoting optimal wide-area control of power networks," *IEEE Transactions on Power Systems*, vol. 29, no. 5, pp. 2281–2291, 2014.

[12] M. Bazrafshan, N. Gatsis, A. F. Taha, and J. A. Taylor, "Coupling load-following control with opf," *IEEE Transactions on Smart Grid*, vol. 10, no. 3, pp. 2495–2506, 2019.

[13] A. F. Taha, M. Bazrafshan, S. A. Nugroho, N. Gatsis, and J. Qi, "Robust control for renewable-integrated power networks considering input bound constraints and worst case uncertainty measure," *IEEE Transactions on Control of Network Systems*, vol. 6, no. 3, pp. 1210–1222, 2019.

[14] T. Sadamoto, A. Chakrabortty, T. Ishizaki, and J. Imura, "Dynamic modeling, stability, and control of power systems with distributed energy resources: Handling faults using two control methods in tandem," *IEEE Control Systems Magazine*, vol. 39, no. 2, pp. 34–65, 2019.

[15] D. D. Siljak, D. M. Stipanovic, and A. I. Zecevic, "Robust decentralized turbine/governor control using linear matrix inequalities," *IEEE Transactions on Power Systems*, vol. 17, no. 3, pp. 715–722, 2002.

[16] S. Elloumi and E. B. Braiek, "Robust decentralized control for multimachine power systems-the lmi approach," in *IEEE International Conference on Systems, Man and Cybernetics*, vol. 6, 2002, pp. 5 pp. vol.6–.

[17] A. I. Zecevic, G. Neskovic, and D. D. Siljak, "Robust decentralized exciter control with linear feedback," *IEEE Transactions on Power Systems*, vol. 19, no. 2, pp. 1096–1103, 2004.

[18] G. K. Befekadu and I. Erlich, "Robust decentralized controller design for power systems using convex optimization involving lmis," *IFAC Proceedings Volumes*, vol. 38, no. 1, pp. 91–96, 2005, 16th IFAC World Congress.

[19] J. Lian, S. Wang, R. Diao, and Z. Huang, "Decentralized robust control for damping inter-area oscillations in power systems," 2017.

[20] W. Wang and H. Ohmori, "Decentralized robust control for multi-machine power system," *IFAC-PapersOnLine*, vol. 48, no. 30, pp. 155–160, 2015, 9th IFAC Symposium on Control of Power and Energy Systems CPES 2015.

[21] A. K. Singh and B. C. Pal, "Decentralized control of oscillatory dynamics in power systems using an extended lqr," *IEEE Transactions on Power Systems*, vol. 31, no. 3, pp. 1715–1728, 2016.

[22] T. Groß, S. Trenn, and A. Wirsen, "Topological solvability and index characterizations for a common dae power system model," in *2014 IEEE Conference on Control Applications (CCA)*, 2014, pp. 9–14.

[23] ——, "Solvability and stability of a power system dae model," *Systems & Control Letters*, vol. 97, pp. 12–17, 2016.

[24] S. Datta, "Small signal stability criteria for descriptor form power network model," *International Journal of Control*, vol. 93, no. 8, pp. 1817–1825, 2020.

[25] D. Patil, P. Tesi, and S. Trenn, "Indiscernible topological variations in dae networks," *Automatica*, vol. 101, pp. 280–289, 2019.

[26] Guoping Lu, D. W. C. Ho, and L. F. Yeung, "Generalized quadratic stability for perturbated singular systems," in *42nd IEEE International Conference on Decision and Control (IEEE Cat. No.03CH37475)*, vol. 3, 2003, pp. 2413–2418 Vol.3.

[27] P. Di Franco, G. Scarciotti, and A. Astolfi, "Stabilization of differential-algebraic systems with lipschitz nonlinearities via feedback decomposition," in *2019 18th European Control Conference (ECC)*, 2019, pp. 1154–1158.

[28] ——, "Stability of nonlinear differential-algebraic systems via additive identity," *IEEE/CAA Journal of Automatica Sinica*, vol. 7, no. 4, pp. 929–941, 2020.

[29] P. Sauer, M. Pai, and J. Chow, *Power System Dynamics and Stability: With Synchrophasor Measurement and Power System Toolbox*, ser. Wiley - IEEE. Wiley, 2017.

[30] B.-M. Hodge, A. Florita, K. Orwig, D. Lew, and M. Milligan, "Comparison of wind power and load forecasting error distributions," National Renewable Energy Lab.(NREL), Golden, CO (United States), Tech. Rep., 2012.

[31] T. Faulwasser, A. Engelmann, T. Mühlpfordt, and V. Hagenmeyer, "Optimal power flow: an introduction to predictive, distributed and stochastic control challenges," *at - Automatisierungstechnik*, vol. 66, no. 7, pp. 573–589, 2018.

[32] G.-R. Duan, *Analysis and design of descriptor linear systems*. Springer Science & Business Media, 2010, vol. 23.

[33] B. Men, Q. Zhang, X. Li, C. Yang, and Y. Chen, "The stability of linear descriptor systems," *International Journal of Information and Systems Sciences*, vol. 2, no. 3, pp. 362–374, 2006.

[34] M. Grant and S. Boyd, "Graph implementations for nonsmooth convex programs," in *Recent Advances in Learning and Control*, ser. Lecture Notes in Control and Information Sciences, V. Blondel, S. Boyd, and H. Kimura, Eds. Springer-Verlag Limited, 2008, pp. 95–110.

[35] J. Löfberg, "Yalmip : A toolbox for modeling and optimization in matlab," in *In Proceedings of the CACSD Conference*, Taipei, Taiwan, 2004.

[36] E. D. Andersen and K. D. Andersen, *The Mosek Interior Point Optimizer for Linear Programming: An Implementation of the Homogeneous Algorithm*. Boston, MA: Springer US, 2000, pp. 197–232.

[37] R. D. Zimmerman, C. E. Murillo-Sánchez, and R. J. Thomas, "Matpower: Steady-state operations, planning, and analysis tools for power systems research and education," *IEEE Transactions on Power Systems*, vol. 26, no. 1, pp. 12–19, 2011.

[38] A. J. Wood and B. F. Wollenberg, *Power Generation, Operation, and Control*, 3rd ed. John Wiley & Sons, 2012.

[39] Z. Wang, F. Liu, J. Z. F. Pang, S. H. Low, and S. Mei, "Distributed optimal frequency control considering a nonlinear network-preserving model," *IEEE Transactions on Power Systems*, vol. 34, no. 1, pp. 76–86, 2019.

[40] M. V. Khlebnikov, P. S. Shcherbakov, and V. N. Chestnov, "Linear-quadratic regulator. i. a new solution," *Automation and Remote Control*, vol. 76, no. 12, pp. 2143–2155, Dec. 2015.

[41] I. Masubuchi, Y. Kamitane, A. Ohara, and N. Suda, "$\mathcal{H}_\infty$ control for descriptor systems: A matrix inequalities approach," *Automatica*, vol. 33, no. 4, pp. 669 – 673, 1997.

[42] S. Xu and J. Lam, *Robust Control and Filtering of Singular Systems*, ser. Lecture Notes in Control and Information Sciences. Springer Berlin Heidelberg, 2006.

[43] Guoping Lu and D. W. C. Ho, "Full-order and reduced-order observers for lipschitz descriptor systems: the unified lmi approach," *IEEE Transactions on Circuits and Systems II: Express Briefs*, vol. 53, no. 7, pp. 563–567, 2006.

APPENDIX A
DESCRIPTION OF MATRICES IN NDAES (4)

The matrix $\boldsymbol{A}_d$ is constructed as

$$\begin{bmatrix} \boldsymbol{O} & \boldsymbol{I} & \boldsymbol{O} & \boldsymbol{O} \\ \boldsymbol{O} & -\operatorname{Diag}(\boldsymbol{D} \oslash \boldsymbol{M}) & \boldsymbol{O} & \operatorname{Diag}(\boldsymbol{1} \oslash \boldsymbol{M}) \\ \boldsymbol{O} & \boldsymbol{O} & -\boldsymbol{A}_{d(3,3)} & \boldsymbol{O} \\ \boldsymbol{O} & \boldsymbol{A}_{d(4,2)} & \boldsymbol{O} & -\operatorname{Diag}(\boldsymbol{1} \oslash \boldsymbol{T}_{\mathrm{CH}}) \end{bmatrix},$$

in which the two submatrices in $\boldsymbol{A}_d$ are given as

$$\boldsymbol{A}_{d(3,3)} = \operatorname{Diag}(\boldsymbol{x}_{\mathrm{d}} \oslash (\boldsymbol{x}'_{\mathrm{d}} \odot \boldsymbol{T}'_{\mathrm{d0}}))$$
$$\boldsymbol{A}_{d(4,2)} = \operatorname{Diag}(\boldsymbol{1} \oslash (\boldsymbol{R}_{\mathrm{d}} \odot \boldsymbol{T}_{\mathrm{CH}})),$$

and the matrices $\boldsymbol{G}_d$, $\boldsymbol{B}_d$, $\boldsymbol{F}$ are specified as

$$\boldsymbol{G}_d := \begin{bmatrix} \boldsymbol{O} & \boldsymbol{O} \\ \operatorname{Diag}(\boldsymbol{1} \oslash \boldsymbol{M}) & \boldsymbol{O} \\ \boldsymbol{O} & \operatorname{Diag}((\boldsymbol{x}_{\mathrm{d}} - \boldsymbol{x}'_{\mathrm{d}}) \oslash (\boldsymbol{x}'_{\mathrm{d}} \odot \boldsymbol{T}'_{\mathrm{d0}})) \\ \boldsymbol{O} & \boldsymbol{O} \end{bmatrix}$$

$$\boldsymbol{B}_d := \begin{bmatrix} \boldsymbol{O} & \boldsymbol{O} \\ \boldsymbol{O} & \boldsymbol{O} \\ \operatorname{Diag}(\boldsymbol{1} \oslash \boldsymbol{T}'_{\mathrm{d0}}) & \boldsymbol{O} \\ \boldsymbol{O} & \operatorname{Diag}(\boldsymbol{1} \oslash \boldsymbol{T}_{\mathrm{CH}}) \end{bmatrix}$$

$$\boldsymbol{h} := \begin{bmatrix} \boldsymbol{1} \\ \boldsymbol{D} \oslash \boldsymbol{M} \\ \boldsymbol{O} \\ \boldsymbol{1} \oslash (\boldsymbol{R}_{\mathrm{d}} \odot \boldsymbol{T}_{\mathrm{CH}}) \end{bmatrix}.$$

The function $\boldsymbol{f}_d(\cdot)$ in (4) is given as

$$\boldsymbol{f}_d(\boldsymbol{x}_d, \boldsymbol{x}_a) := \begin{bmatrix} \boldsymbol{P}_{\mathrm{G}} \\ \{v_i \cos(\delta_i - \theta_i)\}_{i \in \mathcal{G}} \end{bmatrix},$$

Next, the matrices $\boldsymbol{A}_a$, $\boldsymbol{G}_a$, and $\boldsymbol{B}_a$ are detailed as

$$\boldsymbol{A}_a = \begin{bmatrix} -\boldsymbol{I} & \boldsymbol{O} \\ \boldsymbol{A}_p & \boldsymbol{O} \end{bmatrix}, \ \boldsymbol{G}_a = \operatorname{Blkdiag}\left(\tilde{\boldsymbol{G}}_a, \boldsymbol{I}\right), \ \boldsymbol{B}_a = \begin{bmatrix} \boldsymbol{O} \\ \boldsymbol{B}_p \end{bmatrix},$$

where $\boldsymbol{A}_p := \begin{bmatrix} -\boldsymbol{I} & \boldsymbol{O} \end{bmatrix}^\top$ and $\tilde{\boldsymbol{G}}_a$ is detailed as

$$\tilde{\boldsymbol{G}}_a := \begin{bmatrix} \operatorname{Diag}(\boldsymbol{1} \oslash \boldsymbol{x}'_{\mathrm{d}}) & \boldsymbol{O} \\ \tilde{\boldsymbol{G}}_{a(1,2)} & \boldsymbol{O} \\ \boldsymbol{O} & \operatorname{Diag}(\boldsymbol{1} \oslash \boldsymbol{x}'_{\mathrm{d}}) \\ \boldsymbol{O} & -\tilde{\boldsymbol{G}}_{a(2,4)} \\ \boldsymbol{O} & \tilde{\boldsymbol{G}}_{a(2,5)} \end{bmatrix}^\top,$$

with $\tilde{\boldsymbol{G}}_{a(1,2)} := \operatorname{Diag}((\boldsymbol{x}'_{\mathrm{d}} - \boldsymbol{x}_{\mathrm{q}}) \oslash (2\boldsymbol{x}'_{\mathrm{d}} \odot \boldsymbol{x}_{\mathrm{q}}))$, $\tilde{\boldsymbol{G}}_{a(2,4)} := \operatorname{Diag}((\boldsymbol{x}'_{\mathrm{d}} + \boldsymbol{x}_{\mathrm{q}}) \oslash (2\boldsymbol{x}'_{\mathrm{d}} \odot \boldsymbol{x}_{\mathrm{q}}))$, and $\tilde{\boldsymbol{G}}_{a(2,5)} := \tilde{\boldsymbol{G}}_{a(1,2)}$. The matrix $\boldsymbol{B}_p$ is a binary matrix having 1 in each of its elements corresponding to buses that are connected with renewables and/or load—the entries of $\boldsymbol{B}_p$ are set to be zero otherwise. The function $\boldsymbol{f}_a(\cdot)$ in (4) is constructed as

$$\boldsymbol{f}_a(\boldsymbol{x}_d, \boldsymbol{x}_a) := \begin{bmatrix} \{E'_i v_i \sin(\delta_i - \theta_i)\}_{i \in \mathcal{G}} \\ \{v_i^2 \sin(2(\delta_i - \theta_i))\}_{i \in \mathcal{G}} \\ \{E'_i v_i \cos(\delta_i - \theta_i)\}_{i \in \mathcal{G}} \\ \{v_i^2\}_{i \in \mathcal{G}} \\ \{v_i^2 \cos(2(\delta_i - \theta_i))\}_{i \in \mathcal{G}} \\ \left\{\sum_{j=1}^N v_i v_j (G_{ij} \cos\theta_{ij} + B_{ij} \sin\theta_{ij})\right\}_{i \in \mathcal{G}} \\ \left\{\sum_{j=1}^N v_i v_j (G_{ij} \sin\theta_{ij} - B_{ij} \cos\theta_{ij})\right\}_{i \in \mathcal{G}} \\ \left\{\sum_{j=1}^N v_i v_j (G_{ij} \cos\theta_{ij} + B_{ij} \sin\theta_{ij})\right\}_{i \in \mathcal{N} \setminus \mathcal{G}} \\ \left\{\sum_{j=1}^N v_i v_j (G_{ij} \sin\theta_{ij} - B_{ij} \cos\theta_{ij})\right\}_{i \in \mathcal{N} \setminus \mathcal{G}} \end{bmatrix}.$$

APPENDIX B
PROOF OF THEOREM 1

The following lemma is presented first due to its importance in the proof of Theorem 1.

Lemma 1. *For any matrix $\boldsymbol{M} \in \mathbb{R}^{r \times s}$ with $r < s$ and scalars $a, b \in \mathbb{R}_{++}$, the following holds*

$$\boldsymbol{M}^\top (a\boldsymbol{M}\boldsymbol{M}^\top + b\boldsymbol{I})^{-1} \boldsymbol{M} - a\boldsymbol{I} \preceq 0. \tag{14}$$

Proof. Consider the singular value decomposition of $\boldsymbol{M}$ written as $\boldsymbol{M} = \boldsymbol{U} \begin{bmatrix} \boldsymbol{\Lambda} & \boldsymbol{O} \end{bmatrix} \boldsymbol{V}^\top$ where $\boldsymbol{\Lambda} \in \mathbb{R}^{r \times r}$ is a diagonal matrix populating all singular values of $\boldsymbol{M}$ while $\boldsymbol{U} \in \mathbb{R}^{r \times r}$ and $\boldsymbol{V} \in \mathbb{R}^{s \times s}$ are two orthogonal matrices. As the term $a\boldsymbol{M}\boldsymbol{M}^\top + b\boldsymbol{I}$ for positive scalars a and b can be written as

$$a\boldsymbol{M}\boldsymbol{M}^\top + b\boldsymbol{I} = \boldsymbol{U} \left(a\boldsymbol{\Lambda}^2 + b\boldsymbol{I}\right) \boldsymbol{U}^\top,$$

then it can be shown that the term $\boldsymbol{M}^\top (a\boldsymbol{M}\boldsymbol{M}^\top + b\boldsymbol{I})^{-1} \boldsymbol{M}$ is equal to

$$\boldsymbol{V} \left(\operatorname{Blkdiag}\left(a\boldsymbol{\Lambda}^2 \left(\boldsymbol{\Lambda}^2 + \tfrac{b}{a}\boldsymbol{I}\right)^{-1}, \boldsymbol{O}\right)\right) \boldsymbol{V}^\top.$$

Nevertheless, since the inequality $\left(\boldsymbol{\Lambda}^2 + \frac{b}{a}\boldsymbol{I}\right)^{-1} \preceq \boldsymbol{\Lambda}^{-2}$ implies $a\boldsymbol{\Lambda}^2 \left(\boldsymbol{\Lambda}^2 + \frac{b}{a}\boldsymbol{I}\right)^{-1} \preceq a\boldsymbol{I}$, (14) is inferred. ■

Now we are ready to prove Theorem 1, which is decomposed into four parts:

(a) Showing that the dynamic state is asymptotically stable.
(b) Demonstrating that the matrices associated with the Lyapunov function are nonsingular.
(c) Showing that the algebraic state is asymptotically stable.
(d) Establishing the matrix inequalities in (11).

(a): Let $V : \mathbb{R}^{n_d} \to \mathbb{R}_+$ be a Lyapunov function candidate such that $V(t) = \boldsymbol{x}_d^\top \boldsymbol{E}_d^\top \boldsymbol{P}_1 \boldsymbol{x}_d$ where $\boldsymbol{P}_1 \in \mathbb{R}^{n_d \times n_d}$ is assumed (for now) to be nonsingular and $\boldsymbol{E}_d^\top \boldsymbol{P}_1 = \boldsymbol{P}_1^\top \boldsymbol{E}_d \succ 0$. The time derivative of $V(\cdot)$ is equivalent to

$$\begin{aligned} \dot{V}(t) = &\left(\bar{\boldsymbol{A}}_d \boldsymbol{x}_d + \boldsymbol{G}_d \boldsymbol{f}_d(\boldsymbol{x}_d, \boldsymbol{x}_a)\right)^\top \boldsymbol{P}_1 \boldsymbol{x}_d \\ &+ \boldsymbol{x}_d^\top \boldsymbol{P}_1^\top \left(\bar{\boldsymbol{A}}_d \boldsymbol{x}_d + \boldsymbol{G}_d \boldsymbol{f}_d(\boldsymbol{x}_d, \boldsymbol{x}_a)\right), \end{aligned} \tag{15}$$

where $\bar{\boldsymbol{A}}_d^d := \boldsymbol{A}_d + \boldsymbol{B}_d \boldsymbol{K}_d$. For any DAE of index H, then for any function $\boldsymbol{\Gamma}_i(\cdot)$, $i \in \{0, 1, \ldots, H-1\}$, we have [28]

$$\sum_{i=0}^{H-1} \boldsymbol{\Gamma}_i(\boldsymbol{x}_d, \boldsymbol{x}_a) \frac{d^i \boldsymbol{h}(\boldsymbol{x}_d, \boldsymbol{x}_a)}{dt^i} = 0, \ \forall \boldsymbol{x}_d \in \boldsymbol{\mathcal{X}}_d, \ \boldsymbol{x}_a \in \boldsymbol{\mathcal{X}}_a, \tag{16}$$

where the function $\boldsymbol{h}(\cdot)$ represents all terms in right-hand side of (8b). Since the DAE is of index-one, thanks to Assumption 2, then the following choice of $\boldsymbol{\Gamma}_0(\boldsymbol{x}_d, \boldsymbol{x}_a)$ such that

$$\boldsymbol{\Gamma}_0(\boldsymbol{x}_d, \boldsymbol{x}_a) := \boldsymbol{x}_d^\top \boldsymbol{P}_2^\top + \boldsymbol{x}_a^\top \boldsymbol{P}_3^\top, \tag{17}$$

for some $\boldsymbol{P}_2 \in \mathbb{R}^{n_a \times n_d}$ and $\boldsymbol{P}_3 \in \mathbb{R}^{n_a \times n_a}$ is sufficient. Adding (16) to (15), using (17), allows (15) to be expressed into

$$\begin{aligned} \dot{V}(t) = &\left(\bar{\boldsymbol{A}}_d \boldsymbol{x}_d + \boldsymbol{G}_d \boldsymbol{f}_d(\boldsymbol{x}_d, \boldsymbol{x}_a)\right)^\top \boldsymbol{P}_1 \boldsymbol{x}_d \\ &+ \boldsymbol{x}_d^\top \boldsymbol{P}_1^\top \left(\bar{\boldsymbol{A}}_d \boldsymbol{x}_d + \boldsymbol{G}_d \boldsymbol{f}_d(\boldsymbol{x}_d, \boldsymbol{x}_a)\right) \\ &+ \left(\boldsymbol{A}_a \boldsymbol{x}_a + \boldsymbol{G}_a \boldsymbol{f}_a(\boldsymbol{x}_d, \boldsymbol{x}_a)\right)^\top (\boldsymbol{P}_2 \boldsymbol{x}_d + \boldsymbol{P}_3 \boldsymbol{x}_a) \\ &+ \left(\boldsymbol{x}_d^\top \boldsymbol{P}_2^\top + \boldsymbol{x}_a^\top \boldsymbol{P}_3^\top\right) \left(\boldsymbol{A}_a \boldsymbol{x}_a + \boldsymbol{G}_a \boldsymbol{f}_a(\boldsymbol{x}_d, \boldsymbol{x}_a)\right). \end{aligned} \tag{18}$$

From (9), the following inequalities are obtained

$$\begin{aligned} 0 \le &\epsilon \boldsymbol{x}_d^\top \bar{\boldsymbol{H}}_d \boldsymbol{x}_d - \epsilon \boldsymbol{f}_d(\boldsymbol{x}_d, \boldsymbol{x}_a)^\top \boldsymbol{f}_d(\boldsymbol{x}_d, \boldsymbol{x}_a) \\ &+ \epsilon \boldsymbol{x}_a^\top \bar{\boldsymbol{H}}_a \boldsymbol{x}_a - \epsilon \boldsymbol{f}_a(\boldsymbol{x}_d, \boldsymbol{x}_a)^\top \boldsymbol{f}_a(\boldsymbol{x}_d, \boldsymbol{x}_a), \end{aligned} \tag{19}$$

for a scalar $\epsilon \in \mathbb{R}_{++}$. Next, adding (19) to the right-hand side of (18) yields the inequality

$$\dot{V}(t) \leq \boldsymbol{\omega}^\top \boldsymbol{\Omega} \boldsymbol{\omega}, \tag{20}$$

where $\boldsymbol{\omega} := \begin{bmatrix} \boldsymbol{x}_d^\top & \boldsymbol{x}_a^\top & \boldsymbol{f}_d^\top(\boldsymbol{x}_d, \boldsymbol{x}_a) & \boldsymbol{f}_a^\top(\boldsymbol{x}_d, \boldsymbol{x}_a) \end{bmatrix}^\top$ and

$$\boldsymbol{\Omega} := \begin{bmatrix} \boldsymbol{\Omega}_{(1,1)} & * & * & * \\ \boldsymbol{A}_a^\top \boldsymbol{P}_2 & \boldsymbol{\Omega}_{(2,2)} & * & * \\ \boldsymbol{G}_d^\top \boldsymbol{P}_1 & \boldsymbol{O} & -\epsilon \boldsymbol{I} & * \\ \boldsymbol{G}_a^\top \boldsymbol{P}_2 & \boldsymbol{G}_a^\top \boldsymbol{P}_3 & \boldsymbol{O} & -\epsilon \boldsymbol{I} \end{bmatrix}, \tag{21}$$

where the block diagonal matrices are specified as

$$\boldsymbol{\Omega}_{(1,1)} := \bar{\boldsymbol{A}}_d^\top \boldsymbol{P}_1 + \boldsymbol{P}_1^\top \bar{\boldsymbol{A}}_d + \epsilon \bar{\boldsymbol{H}}_d$$
$$\boldsymbol{\Omega}_{(2,2)} := \boldsymbol{A}_a^\top \boldsymbol{P}_3 + \boldsymbol{P}_3^\top \boldsymbol{A}_a + \epsilon \bar{\boldsymbol{H}}_a.$$

It will be demonstrated in the sequel that the system of NDAEs (7) is asymptotically stable around the origin if $\boldsymbol{\omega}^\top \boldsymbol{\Omega} \boldsymbol{\omega} < 0$ for any $\boldsymbol{\omega} \neq 0$. Realize that this condition is equivalent to $\boldsymbol{\Omega} \prec 0$. By using Raleigh inequality, we have

$$\boldsymbol{\omega}^\top \boldsymbol{\Omega} \boldsymbol{\omega} \leq \lambda_{\max}(\boldsymbol{\Omega}) \|\boldsymbol{\omega}\|_2^2. \tag{22}$$

Since the following also holds

$$\|\boldsymbol{\omega}\|_2^2 \leq (1 + \lambda_{\max}(\bar{\boldsymbol{H}}_d)) \|\boldsymbol{x}_d\|_2^2 + (1 + \lambda_{\max}(\bar{\boldsymbol{H}}_a)) \|\boldsymbol{x}_a\|_2^2,$$

thanks to (9), then from (22) one can simply obtain

$$\boldsymbol{\omega}^\top \boldsymbol{\Omega} \boldsymbol{\omega} \leq -\eta_1 \|\boldsymbol{x}_d\|_2^2 - \eta_2 \|\boldsymbol{x}_a\|_2^2, \tag{23}$$

where in (23), $\eta_1, \eta_2 \in \mathbb{R}_{++}$ defined as $\eta_1 := -\lambda_{\max}(\boldsymbol{\Omega})(1 + \lambda_{\max}(\bar{\boldsymbol{H}}_d))$ and $\eta_2 := -\lambda_{\max}(\boldsymbol{\Omega})(1 + \lambda_{\max}(\bar{\boldsymbol{H}}_a))$. Now, as $\boldsymbol{P}_1$ being nonsingular implies

$$-\eta_1 \|\boldsymbol{x}_d\|_2^2 - \eta_2 \|\boldsymbol{x}_a\|_2^2 \leq -\eta_1 \lambda_{\max}^{-1}(\boldsymbol{E}_d^\top \boldsymbol{P}_1) V(t),$$

then (20) and (23) lead to

$$\begin{aligned} \dot{V}(t) &\leq -\eta_1 \lambda_{\max}^{-1}(\boldsymbol{E}_d^\top \boldsymbol{P}_1) V(t) \\ \Rightarrow \int_{t_0}^{t} \frac{1}{V(\tau)} dV(\tau) &\leq \int_{t_0}^{t} -\eta_1 \lambda_{\max}^{-1}(\boldsymbol{E}_d^\top \boldsymbol{P}_1)\, d\tau \\ \Leftrightarrow V(t) &\leq e^{-\eta_1 \lambda_{\max}^{-1}(\boldsymbol{E}_d^\top \boldsymbol{P}_1)(t-t_0)} V(t_0). \end{aligned} \tag{24}$$

Since $\|\boldsymbol{x}_d\|_2^2 \leq \lambda_{\min}^{-1}(\boldsymbol{E}_d^\top \boldsymbol{P}_1) V(t)$, then from (24) we obtain

$$\|\boldsymbol{x}_d(t)\|_2 \leq \psi e^{-\frac{1}{2}\eta_1 \lambda_{\max}^{-1}(\boldsymbol{E}_d^\top \boldsymbol{P}_1)(t-t_0)} \|\boldsymbol{x}_d(t_0)\|_2, \tag{25}$$

where $\psi > 0$ is a residual term given as

$$\psi := \sqrt{\lambda_{\min}^{-1}\left(\boldsymbol{E}_d^\top \boldsymbol{P}_1\right) \lambda_{\max}\left(\boldsymbol{E}_d^\top \boldsymbol{P}_1\right)}.$$

The inequality (25) implies that $\|\boldsymbol{x}_d(t)\|_2 \to 0$ as $t \to \infty$.

(b): Secondly, since we require $\boldsymbol{\Omega} \prec 0$, then it holds that the pair $\left(\text{Blkdiag}(\boldsymbol{E}_d, \boldsymbol{O}), \text{Blkdiag}(\bar{\boldsymbol{A}}_d, \boldsymbol{A}_a)\right)$ is both regular and impulse-free [41]. As such, there exist nonsingular matrices $\boldsymbol{M}, \boldsymbol{N} \in \mathbb{R}^{n_x \times n_x}$ where $n_x := n_d + n_a$ such that [32]

$$\tilde{\boldsymbol{E}} = \boldsymbol{M} \begin{bmatrix} \boldsymbol{E}_d & \boldsymbol{O} \\ \boldsymbol{O} & \boldsymbol{O} \end{bmatrix} \boldsymbol{N} = \begin{bmatrix} \boldsymbol{I} & \boldsymbol{O} \\ \boldsymbol{O} & \boldsymbol{O} \end{bmatrix} \tag{26a}$$

$$\tilde{\boldsymbol{A}} = \boldsymbol{M} \begin{bmatrix} \bar{\boldsymbol{A}}_d & \boldsymbol{O} \\ \boldsymbol{O} & \boldsymbol{A}_a \end{bmatrix} \boldsymbol{N} = \begin{bmatrix} \tilde{\boldsymbol{A}}_d & \boldsymbol{O} \\ \boldsymbol{O} & \boldsymbol{I} \end{bmatrix}, \tag{26b}$$

with $\boldsymbol{M}$, $\boldsymbol{N}$ partitioned as follows

$$\boldsymbol{M} = \begin{bmatrix} \boldsymbol{M}_1^\top & \boldsymbol{M}_2^\top \end{bmatrix}^\top, \quad \boldsymbol{N} = \begin{bmatrix} \boldsymbol{N}_1 & \boldsymbol{N}_2 \end{bmatrix},$$

where $\boldsymbol{M}_1 \in \mathbb{R}^{n_d \times n_x}$, $\boldsymbol{M}_2 \in \mathbb{R}^{n_a \times n_x}$, $\boldsymbol{N}_1 \in \mathbb{R}^{n_x \times n_d}$, $\boldsymbol{N}_2 \in \mathbb{R}^{n_x \times n_a}$. In addition, define the transformed state $\tilde{\boldsymbol{x}} \in \mathbb{R}^{n_x}$ as

$$\tilde{\boldsymbol{x}} = \begin{bmatrix} \tilde{\boldsymbol{x}}_d \\ \tilde{\boldsymbol{x}}_a \end{bmatrix} := \boldsymbol{N}^{-1} \begin{bmatrix} \boldsymbol{x}_d \\ \boldsymbol{x}_a \end{bmatrix}, \quad \tilde{\boldsymbol{x}}_d \in \mathbb{R}^{n_d}, \ \tilde{\boldsymbol{x}}_a \in \mathbb{R}^{n_a}. \tag{27}$$

It then can be directly shown the existence of matrices $\tilde{\boldsymbol{P}}_1 \in \mathbb{R}^{n_d \times n_d}$, $\tilde{\boldsymbol{P}}_2 \in \mathbb{R}^{n_d \times n_a}$, and $\tilde{\boldsymbol{P}}_3 \in \mathbb{R}^{n_a \times n_a}$ such that

$$\begin{bmatrix} \tilde{\boldsymbol{P}}_1 & \boldsymbol{O} \\ \tilde{\boldsymbol{P}}_2 & \tilde{\boldsymbol{P}}_3 \end{bmatrix} = \boldsymbol{M}^{-\top} \begin{bmatrix} \boldsymbol{P}_1 & \boldsymbol{O} \\ \boldsymbol{P}_2 & \boldsymbol{P}_3 \end{bmatrix} \boldsymbol{N}, \tag{28}$$

with $\tilde{\boldsymbol{P}}_1$ is symmetric. Since $V(t) = \boldsymbol{x}_d^\top \boldsymbol{E}_d^\top \boldsymbol{P}_1 \boldsymbol{x}_d = \tilde{\boldsymbol{x}}_d^\top \tilde{\boldsymbol{P}}_1 \tilde{\boldsymbol{x}}_d$, then $\tilde{\boldsymbol{P}}_1 \succ 0$. Using Schur complement, it is straightforward to show that $\boldsymbol{\Omega} \prec 0$ is equivalent to $\tilde{\boldsymbol{\Omega}} \prec 0$ where $\tilde{\boldsymbol{\Omega}}$ is defined as

$$\tilde{\boldsymbol{\Omega}} := \tilde{\boldsymbol{A}}^\top \tilde{\boldsymbol{P}} + \tilde{\boldsymbol{P}}^\top \tilde{\boldsymbol{A}} + \epsilon \boldsymbol{N}^\top \bar{\boldsymbol{H}}^\top \boldsymbol{N} + \epsilon \tilde{\boldsymbol{P}}^\top \boldsymbol{M} \boldsymbol{G} \boldsymbol{G}^\top \boldsymbol{M}^\top \tilde{\boldsymbol{P}},$$

where $\bar{\boldsymbol{H}} := \text{Blkdiag}(\bar{\boldsymbol{H}}_d, \bar{\boldsymbol{H}}_a)$, $\boldsymbol{G} := \text{Blkdiag}(\bar{\boldsymbol{G}}_d, \bar{\boldsymbol{G}}_a)$ and $\tilde{\boldsymbol{P}}$ is equal to the left-hand side of (28). It can be shown from the $(2,2)$ block of $\tilde{\boldsymbol{\Omega}}$ that $\tilde{\boldsymbol{\Omega}} \prec 0$ implies $\tilde{\boldsymbol{P}}_3 + \tilde{\boldsymbol{P}}_3^\top \prec 0$. Now let us define a matrix measure function [42] $\nu : \mathbb{R}^{n_a \times n_a} \to \mathbb{R}$ as follows

$$\nu\left(\tilde{\boldsymbol{P}}_3\right) := \lim_{\theta \to 0^+} \frac{\left\|\boldsymbol{I} + \theta \tilde{\boldsymbol{P}}_3\right\|_2 - 1}{\theta}.$$

Due to Lemma 2.4 in [42], then the inequality below holds

$$\lambda_{\max}\left(\tilde{\boldsymbol{P}}_3\right) \leq \nu\left(\tilde{\boldsymbol{P}}_3\right) = \frac{1}{2} \lambda_{\max}\left(\tilde{\boldsymbol{P}}_3 + \tilde{\boldsymbol{P}}_3^\top\right). \tag{29}$$

The above inequality suggests that $\tilde{\boldsymbol{P}}_3$ is nonsingular as $\tilde{\boldsymbol{P}}_3 + \tilde{\boldsymbol{P}}_3^\top \prec 0$ infers that the right-hand side of (29) is negative. This shows that the matrix $\tilde{\boldsymbol{P}}$ defined in (28) is nonsingular. However, since $\boldsymbol{M}, \boldsymbol{N}$ are also nonsingular, then it can be inferred from (28) that $\boldsymbol{P}_1$ and $\boldsymbol{P}_3$ are nonsingular—this confirms the validity of the previous assumption.

(c): Thirdly, from the fact that the $(2,2)$ block of $\tilde{\boldsymbol{\Omega}}$ is negative definite, then for a constant $\delta > 0$, we have

$$\tilde{\boldsymbol{P}}_3 + \tilde{\boldsymbol{P}}_3^\top + \epsilon \boldsymbol{N}_2^\top \bar{\boldsymbol{H}} \boldsymbol{N}_2 + \tilde{\boldsymbol{P}}_3^\top \boldsymbol{\Xi} \tilde{\boldsymbol{P}}_3 \prec 0, \tag{30}$$

where $\boldsymbol{\Xi} := \epsilon \boldsymbol{M}_2 \boldsymbol{G} \boldsymbol{G}^\top \boldsymbol{M}_2 + \delta \boldsymbol{I}$ is nonsingular. Notice that (30) can be written as [43]

$$\left(\tilde{\boldsymbol{P}}_3 + \boldsymbol{\Xi}^{-1}\right)^\top \boldsymbol{\Xi} \left(\tilde{\boldsymbol{P}}_3 + \boldsymbol{\Xi}^{-1}\right) - \boldsymbol{\Xi}^{-1} + \epsilon \boldsymbol{N}_2^\top \bar{\boldsymbol{H}} \boldsymbol{N}_2 \prec 0.$$

Since we have $\left(\tilde{\boldsymbol{P}}_3 + \boldsymbol{\Xi}^{-1}\right)^\top \boldsymbol{\Xi} \left(\tilde{\boldsymbol{P}}_3 + \boldsymbol{\Xi}^{-1}\right) \succ 0$, then from the above equation, there exists $\zeta > 0$ such that [43]

$$(\epsilon + \zeta) \boldsymbol{N}_2^\top \bar{\boldsymbol{H}} \boldsymbol{N}_2 - \boldsymbol{\Xi}^{-1} \prec 0. \tag{31}$$

It then can be shown from (31) and Lemma 1 that

$$\begin{aligned} &\left\|\bar{\boldsymbol{H}}^{\frac{1}{2}} \boldsymbol{N}_2 \boldsymbol{M}_2 \boldsymbol{G} \boldsymbol{f}(\boldsymbol{x}_d, \boldsymbol{x}_a)\right\|_2^2 \\ &\quad \leq \frac{1}{\epsilon + \zeta} \boldsymbol{f}^\top(\boldsymbol{x}_d, \boldsymbol{x}_a) \boldsymbol{G}^\top \boldsymbol{M}_2^\top \boldsymbol{\Xi}^{-1} \boldsymbol{M}_2 \boldsymbol{G} \boldsymbol{f}(\boldsymbol{x}_d, \boldsymbol{x}_a) \\ &\quad \leq \frac{\epsilon}{\epsilon + \zeta} \boldsymbol{f}^\top(\boldsymbol{x}_d, \boldsymbol{x}_a) \boldsymbol{f}(\boldsymbol{x}_d, \boldsymbol{x}_a), \end{aligned}$$

where $\boldsymbol{f}(\boldsymbol{x}_d, \boldsymbol{x}_a) := \begin{bmatrix} \boldsymbol{f}_d^\top(\boldsymbol{x}_d, \boldsymbol{x}_a) & \boldsymbol{f}_a^\top(\boldsymbol{x}_d, \boldsymbol{x}_a) \end{bmatrix}^\top$, implying

$$\|\boldsymbol{f}(\boldsymbol{x}_d, \boldsymbol{x}_a)\|_2^2 \leq \frac{\epsilon + \zeta}{\zeta} \left\|\bar{\boldsymbol{H}}^{\frac{1}{2}} \boldsymbol{N}_2\right\|_F^2 \|\tilde{\boldsymbol{x}}_d\|_2^2. \tag{32}$$

Using (32), it is straightforward to show that

$$\|\tilde{\boldsymbol{x}}_a\|_2 \leq \sqrt{\tfrac{\epsilon + \zeta}{\zeta}} \|\boldsymbol{M}_2 \boldsymbol{G}\|_F \left\|\bar{\boldsymbol{H}}^{\frac{1}{2}} \boldsymbol{N}_2\right\|_F \|\tilde{\boldsymbol{x}}_d\|_2,$$

which, according to (25), leads to

$$\|\boldsymbol{x}_a(t)\|_2 \leq \varrho e^{-\frac{1}{2}\eta_1 \lambda_{\max}^{-1}(\boldsymbol{E}_d^\top \boldsymbol{P}_1)(t-t_0)} \|\boldsymbol{x}_d(t_0)\|_2, \tag{33}$$

where $\varrho > 0$ is a residual term. The inequality (33) indicates that $\|\boldsymbol{x}_a(t)\|_2 \to 0$ as $t \to \infty$.

(d): Finally, since $\boldsymbol{P}_1$ and $\boldsymbol{P}_3$ are nonsingular, we can define $\boldsymbol{Q}_1 \in \mathbb{R}^{n_d \times n_d}$, $\boldsymbol{Q}_2 \in \mathbb{R}^{n_d \times n_a}$, and $\boldsymbol{Q}_3 \in \mathbb{R}^{n_a \times n_a}$ such that

$$\boldsymbol{Q}_1 := \boldsymbol{P}_1^{-1}, \ \boldsymbol{Q}_2 := -\boldsymbol{P}_3^{-1} \boldsymbol{P}_2 \boldsymbol{P}_1^{-1}, \ \boldsymbol{Q}_3 := \boldsymbol{P}_3^{-1}. \tag{34}$$

Using congruence transformation, given the new matrices defined in (34), and applying the Schur complement, the condition $\boldsymbol{\Omega} \prec 0$ can be shown equivalent to (11a) where $\bar{\epsilon} := \frac{1}{\epsilon}$. Note that substituting $\boldsymbol{Q}_1 = \boldsymbol{P}_1^{-1}$ to $\boldsymbol{E}_d^\top \boldsymbol{P}_1 = \boldsymbol{P}_1^\top \boldsymbol{E}_d \succ 0$ establishes (11b). This completes the proof. ■

APPENDIX C
PROOF OF PROPOSITION 1

Notice that, from (26a) and (28), we have

$$\begin{bmatrix} \boldsymbol{E}_d & \boldsymbol{O} \\ \boldsymbol{O} & \boldsymbol{O} \end{bmatrix}^\top = \boldsymbol{N}^{-\top} \begin{bmatrix} \boldsymbol{I} & \boldsymbol{O} \\ \boldsymbol{O} & \boldsymbol{O} \end{bmatrix} \boldsymbol{M}^{-\top}$$

$$\begin{bmatrix} \boldsymbol{P}_1 & \boldsymbol{O} \\ \boldsymbol{P}_2 & \boldsymbol{P}_3 \end{bmatrix}^{-1} = \boldsymbol{N} \begin{bmatrix} \boldsymbol{\Pi}_1 & \boldsymbol{O} \\ \boldsymbol{\Pi}_2 & \boldsymbol{\Pi}_3 \end{bmatrix} \boldsymbol{M}^{-\top},$$

where $\boldsymbol{\Pi}_1 := \tilde{\boldsymbol{P}}_1^{-1}$, $\boldsymbol{\Pi}_2 := -\tilde{\boldsymbol{P}}_3^{-1}\tilde{\boldsymbol{P}}_2\tilde{\boldsymbol{P}}_1^{-1}$, and $\boldsymbol{\Pi}_3 := \tilde{\boldsymbol{P}}_3^{-1}$. The second equation can be written as

$$\begin{aligned} \begin{bmatrix} \boldsymbol{P}_1 & \boldsymbol{O} \\ \boldsymbol{P}_2 & \boldsymbol{P}_3 \end{bmatrix}^{-1} &= \boldsymbol{N} \begin{bmatrix} \boldsymbol{\Pi}_1 & \boldsymbol{O} \\ \boldsymbol{O} & \boldsymbol{I} \end{bmatrix} \begin{bmatrix} \boldsymbol{I} & \boldsymbol{O} \\ \boldsymbol{O} & \boldsymbol{O} \end{bmatrix} \boldsymbol{M}^{-\top} \\ &\quad + \boldsymbol{N} \begin{bmatrix} \boldsymbol{O} \\ \boldsymbol{I} \end{bmatrix} \begin{bmatrix} \boldsymbol{\Pi}_2 & \boldsymbol{\Pi}_3 \end{bmatrix} \boldsymbol{M}^{-\top}. \end{aligned} \tag{35}$$

Since $\boldsymbol{N}^\top \mathrm{Blkdiag}\left(\boldsymbol{E}_d^\top, \boldsymbol{O}\right) \boldsymbol{M}^\top \begin{bmatrix} \boldsymbol{O} & \boldsymbol{I} \end{bmatrix} = 0$, then there exists a full rank matrix $\boldsymbol{\Phi} \in \mathbb{R}^{n_a \times n_a}$ such that [26]

$$\boldsymbol{\Phi} \begin{bmatrix} \boldsymbol{O} & \boldsymbol{I} \end{bmatrix} \boldsymbol{N}^\top \begin{bmatrix} \boldsymbol{E}_d & \boldsymbol{O} \\ \boldsymbol{O} & \boldsymbol{O} \end{bmatrix}^\top = 0,$$

which allows (35) to be expressed as

$$\begin{aligned} \begin{bmatrix} \boldsymbol{P}_1 & \boldsymbol{O} \\ \boldsymbol{P}_2 & \boldsymbol{P}_3 \end{bmatrix}^{-1} &= \boldsymbol{N} \begin{bmatrix} \boldsymbol{\Pi}_1 & \boldsymbol{O} \\ \boldsymbol{O} & \boldsymbol{I} \end{bmatrix} \boldsymbol{N}^\top \boldsymbol{N}^{-\top} \begin{bmatrix} \boldsymbol{I} & \boldsymbol{O} \\ \boldsymbol{O} & \boldsymbol{O} \end{bmatrix} \boldsymbol{M}^{-\top} \\ &\quad + \boldsymbol{N} \begin{bmatrix} \boldsymbol{O} \\ \boldsymbol{I} \end{bmatrix} \boldsymbol{\Phi}^\top \boldsymbol{\Phi}^{-\top} \begin{bmatrix} \boldsymbol{\Pi}_2 & \boldsymbol{\Pi}_3 \end{bmatrix} \boldsymbol{M}^{-\top}. \end{aligned}$$

Following [26], it is not difficult to show that the above ensures the existence of matrices $\boldsymbol{X}_1 \in \mathbb{S}_{++}^{n_d}$, $\boldsymbol{X}_2 \in \mathbb{R}^{n_a \times n_d}$, $\boldsymbol{R} \in \mathbb{R}^{n_a \times n_a}$, and $\boldsymbol{Y} \in \mathbb{R}^{n_d \times n_a}$ such that

$$\boldsymbol{Q}_1 = \boldsymbol{X}_1 \boldsymbol{E}_d^\top, \quad \boldsymbol{Q}_2 = \boldsymbol{X}_2 \boldsymbol{E}_d^\top + \boldsymbol{Y}, \quad \boldsymbol{Q}_3 = \boldsymbol{R}. \tag{36}$$

At last, by substituting (36) to (11a) and defining $\boldsymbol{W} := \boldsymbol{K}_d \boldsymbol{X}_1$ for a matrix $\boldsymbol{W} \in \mathbb{R}^{n_u \times n_d}$ (12) is established. Since (36) indeed satisfies (11b), then we are done. ■

Sebastian A. Nugroho received the B.S. and M.S. degrees in Electrical Engineering from Institut Teknologi Bandung, Indonesia in 2012 and 2014 and the Ph.D. degree from the University of Texas at San Antonio (UTSA) in 2021. He is currently a Postdoctoral Research Fellow at the Department of Electrical Engineering and Computer Science, University of Michigan, Ann Arbor. His primary research interests are control theory and engineering optimization with applications to energy systems and transportation networks. While working towards his Ph.D. at UTSA, he received several awards including the Valero Ph.D. Competitive Research Scholarship Awards (2017-2019), the Outstanding Graduate Research Awards (2019), and the Pioneer Competitive Research Scholarship (2020).

Ahmad F. Taha is an associate professor with the Department of Civil and Environmental Engineering at Vanderbilt University in Nashville, Tennessee. He received the B.E. and Ph.D. degrees in Electrical and Computer Engineering from the American University of Beirut, Lebanon in 2011 and Purdue University, West Lafayette, Indiana in 2015. Prior to joining Vanderbilt, Taha was an assistant professor with the University of Texas at San Antonio. Dr. Taha is interested in understanding how complex cyber-physical systems (CPS) operate, behave, and misbehave. His research focus includes optimization, control, and security of CPSs with applications to power, water, and transportation networks. Dr. Taha is an editor of IEEE Transactions on Smart Grid, was the chief editor of the IEEE Control Systems Society (CSS) Electronic Letter (E-Letter), and the current co-editor of the CSS StateSpace Forum.